Engineering Fracture Mechanics 318 (2025) 110963

Contents lists available at ScienceDirect

Engineering Fracture Mechanics

journal homepage: www.elsevier.com/locate/engfracmech

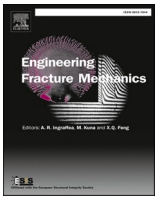

Prediction of the full debonding process of mixed-adhesive FRP-to-substrate joints through a new analytical method

Hugo C. Biscaia [a,b,*], Dilum Fernando [c], Jian-Guo Dai [d]

[a] UNIDEMI, Department of Mechanical and Industrial Engineering, NOVA School of Science and Technology, 2829-516 Caparica, Portugal
[b] Laboratório Associado de Sistemas Inteligentes, LASI, 4800-058 Guimarães, Portugal
[c] School of Engineering, The University of Edinburgh, Edinburgh, UK
[d] Department of Architecture and Civil Engineering, City University of Hong Kong, Hong Kong, China

ARTICLE INFO

Keywords:
FRP composites
Mixed-adhesives
Analytical model
Debonding process
Single-lap shear test

ABSTRACT

Rehabilitation and retrofitting of existing structures using externally bonded fibre-reinforced polymers (FRP) have become increasingly popular. A common failure mode in such strengthened systems is the debonding of the FRP laminate from the substrate. To address this, various techniques have been developed to prevent or delay debonding failures. One such approach is the use of two adhesives with different elastic moduli, resulting in a mixed-adhesive joint. This technique is claimed to reduce stress concentrations at the plate ends, thereby delaying or preventing debonding failures. However, a detailed interfacial stress analysis, considering failure initiation and propagation within the bonded joint, has yet to be conducted to fully understand the effects of using a mixed adhesive. To address this gap, the present work proposes an analytical solution to describe the complete debonding process of FRP mixed-adhesive joints under mode II loading. This analytical solution is validated using the Finite Element Method (FEM), and several key parameters for mixed-adhesive joint design are identified. The results indicate that mixed-adhesive joints, compared to single-adhesive joints with a ductile adhesive, exhibit lower maximum load capacities. When the ductile adhesive is used as a loaded-end anchorage in the mixed-adhesive joint, the maximum load is higher than when it is used as an end anchorage. However, this configuration significantly reduces the ductility of the joint with the loaded-end anchorage.

1. Introduction

The use of carbon fibre-reinforced polymers (CFRP) externally bonded to an existing structural material has recently gained a particular increase. Their good strength-to-weight ratio, resistance to corrosion, durability, easy handling, etc., have made them a good alternative to conventional metallic materials. Therefore, CFRP composites have been used to strengthen existing degraded structures. However, the bonding between adherends plays a critical role in the success of the strengthened structure. These externally bonded structures with CFRP composites are prone to debond prematurely, i.e. the CFRP composite tends to debond from the substrate at a low strain level and its strain rupture is barely achieved at the ultimate state. To bypass this premature debonding issue, several researchers have been proposing and testing different ways to anchor the CFRP composite to the substrate. Usually, increasing the CFRP width or

* Corresponding author.
E-mail address: hb@fct.unl.pt (H.C. Biscaia).

https://doi.org/10.1016/j.engfracmech.2025.110963
Received 1 January 2025; Received in revised form 16 February 2025; Accepted 18 February 2025
Available online 19 February 2025

Nomenclature

A_r	is the cross-sectional area of the FRP composite
A_s	is the cross-sectional area of the substrate
B	is the stiffness index of the interface
b_r	is the width of the reinforcement
C_1	is the first constant obtained from integration
C_2	is the second constant obtained from integration
$d_{s,FEM}$	is the data calculated from the FEM at slip s
$d_{s,PAS}$	is the data obtained from the proposed analytical solution at slip s
E_r	is the elastic modulus of the FRP composite
ε_r	is the strain developed in the FRP composite;
ε_{r0}	is the strain developed at the FRP-free end
$\varepsilon_{r\max}$	is the maximum strain developed in the FRP composite
E_s	is the elastic modulus of the substrate
F_0	load transmitted to the spring
G_F	is the mode II fracture energy
λ	is a constant parameter
$k(s)$	stiffness of the spring with a nonlinear behaviour
L_b	is the bonded length
n	is the number of measurements carried out during the simulations of the debonding process between the FRP composite and the substrate
r	is the ratio between the axial stiffness of the FRP composite and the axial stiffness of the substrate
$r_{analytical}$	is the result (maximum load or displacement at maximum load) obtained from the proposed analytical solution
$r_{numerical}$	is the result (maximum load or displacement at maximum load) obtained from the FEM
s	is the interfacial slip
s_0	is the slip at the mechanically anchored FRP composite
s_{Lb}	is the slip at the FRP-loaded end
$s_{\max}$	is the interfacial slip at maximum bond stress
τ_b	is the bond stress
$\tau_{b\max}$	is the maximum bond stress predicted in the bond-slip relationship
t_r	is the thickness of the FRP composite
x	is the longitudinal coordinate parallel with the bond line of the joint

adding steel plates, CFRP spike anchors, CFRP U-wrap jackets, and steel fasteners at the CFRP ends or along the bonded length, can increase the final strength of the joints. However, no rationale to apply any of these anchors has been widely accepted by the scientific community. For instance, the number of steel fasteners or CFRP spike anchors needed to avoid the premature debonding of the CFRP composite remains unclear. Additionally, using these mechanical anchoring techniques is still a bit labour-intensive. Therefore, easier and more efficient alternative ways to delay the CFRP debonding phenomenon are still being pursued.

An alternative suggested by several researchers is the use of mixed-adhesive bonded joints to enhance their strengths [1–5]. As already demonstrated [2], the aim of using two different adhesive types in a bonded joint is to smoothen the bond stress distributions developed in the interface between adherends and, therefore, enhance its strength. In the literature, e.g. [6–9], several examples with single-lap shear tests under a pull-pull configuration can be seen. Completely different adhesive types are used, i.e. with brittle and ductile behaviours. In a pull-pull test, the brittle adhesive is commonly applied at the centre of the joint whereas the ductile adhesive is placed at both ends of the joints. Raphael [10] introduced this solution in the 1960s so the high-stress concentrations developed at the ends of the overlapped bonded joint could be smoothened. The idea was to decrease the high-stress concentration developed at the ends of the joints by using a more ductile and flexible adhesive since they can tolerate higher strains. As a result, the mixed-adhesive joint will have maximum strength and stiffness at the centre of the joint and maximum flexibility and ductility at the ends.

The increase of the final strength of the mixed-adhesive joints can be also increased if a spew fillet is considered at the ends of the joints, e.g. [11–14]. A spew fillet is an excess of adhesive that results from the bonding process between the adherends. Adherends when pressured against each other squeeze a small portion of adhesive at the ends of the overlap [15]. This small portion of adhesive is beneficial for the final strength of the joints since it reduces the shear and peeling stresses at the ends of the bonded joints [15–18]. Another way to reduce the risk of failure due to the development of high peeling stresses at the ends of the joints is to change the geometry of the free ends of the adherends, e.g., by tapering the free ends of the adherends [19] or creating an end rounding adherend [20]. For instance, the work carried out by Bouchikhi et al. [21] on repaired steel beams with CFRP composites allowed them to conclude that the use of a taper as well as mixed adhesives can reduce the magnitude of the interface stresses on the CFRP ends. Thus, the service life of the repaired steel beam can be extended since the risk of CFRP debonding is reduced.

Analytical solutions have been developed to estimate the shear and peeling stresses in the literature, e.g. [22–26] for which only the elastic performance of the joints is assumed. This can be accepted if the adhesive has an elastic brittle behaviour and the interface

between the adhesive and the adherends is considered rigid. However, when adhesives have a ductile behaviour, their nonlinearities should be taken into account and so, the determination of adequate analytical solutions to accurately estimate the failure load of the joints is difficult even when the adhesive-to-adherends interfaces are assumed to be rigid. The pioneering work of Hart and Smith [27] is known to introduce the simulation of a ductile adhesive through an elastic–plastic model with the same strength, rupture strain and strain energy, and showed that using ductile adhesives leads to higher failure loads of the bonded joints.

Other advanced strategies to better simulate the bond performance of bonded joints is, for instance, the introduction of Cohesive Zone Modelling (CZM). Its use to simulate adhesively bonded structures has been growing and it has proven to be quite accurate in its predictions of different bonded joints under different loading conditions, e.g. [28–35]. In the CZM, the adhesive is replaced by a non-thickness material that can reproduce, considering all their nonlinearities, and the characteristics of the separation between adherends. To do so, the local bond behaviour of the joints is defined through traction and shear laws that define their behaviour under three fracture modes (opening, sliding and tearing). Fracture mode II (sliding), is more relevant than mode I (opening) and mode III (tearing) is usually assumed to be similar to mode II. In the case of fracture mode II, its definition is made through a local bond-slip relationship, which is dependent on the adhesive type. Thus, in a CFRP externally bonded to a structural material, brittle adhesives are associated with triangular bond-slip relationships, whilst ductile adhesives are associated with trapezoidal bond-slip relationships [36–38]. Based on these and other types of bond-slip relationships, several closed-form solutions can be found in the literature that describe the bond performance of bonded structures subjected to mechanical loading [39–45], temperature variation [46–50] or the combination of these two [51,52]. However, to the best knowledge of the author, none of these consider the case of using the mixed-adhesive concept.

Within this context, the present work aims to mitigate the lack of knowledge on the bond behaviour of FRP-to-substrate joints with two different adhesives. Based on the CZM, an analytical solution is proposed where brittle and ductile adhesives are considered. In both cases, an exponential bond-slip relationship well-established in the literature [53] is used to approximate the bond-slip relationships derived from a brittle and a ductile adhesive as assumed by Jiang et al. [54]. Different bonded joints are analysed through the proposed analytical solution and compared with a commercial finite element method (FEM) for validation purposes. Further comparisons with other studies with single-adhesive joints with brittle adhesives are also reported. However, since no similar studies were found in the literature, the experimental results were extrapolated for the case of a mixed-adhesive joint. The results suggest that the idea of a mixed-adhesive joint may not be of significance when compared with the single-adhesive joint using a ductile adhesive. However, if a ductile adhesive is used as a loaded-end anchorage rather than an end anchorage, then the former mixed-adhesive joint can achieve a higher load capacity but a lower ductility in displacement.

2. Problem definition

This section presents all the initial assumptions and subsequent analytical solutions needed to describe the full debonding process of a mixed-adhesive joint.

2.1. Follow-up strategy and initial assumptions of the analytical solution

A CFRP-to-steel mixed-adhesive single-lap shear bonded joint as shown in Fig. 1a was chosen for this study. CFRP-to-steel mixed-adhesive bonded joints have two adhesives, an adhesive 1 and an adhesive 2, with different properties. Therefore, the bond line of the joint has two distinct regions with different adhesive types. Usually, the region close to the CFRP-loaded end has a more ductile and flexible adhesive whilst the rest of the region has a stiffer and more brittle adhesive. For the sake of simplicity, the mixed-adhesive joint is replaced by a bonded joint of a single-adhesive (adhesive 1) closer to the loaded end and a nonlinear spring representing the rest of the bond region with adhesive 2. The stiffness of the nonlinear spring is defined as a function of the slip (denoted by s) as $k(s)$. This nonlinear spring aims to reproduce the force-slip behaviour of the left side of the mixed-adhesive joint (see Fig. 1b). The force developed in the nonlinear spring is denoted here as F_0 whereas the load transmitted to the CFRP composite is denoted as F. To define the force-slip (or strain-slip) curve of the joint with a single adhesive with a CFRP-free end should be known. Only then, is possible to assume the single-lap shear test with a nonlinear spring at the left hand of the joint and with adhesive 2.

Hence, before further analytical considerations to describe the full debonding process of the mixed-adhesive joints, the following assumptions are necessary to be made:

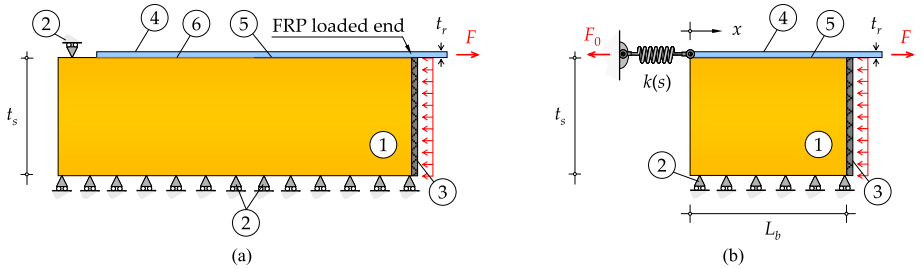

Key: 1 – Substrate; 2 – Roller support; 3 – Steel reaction plate; 4 – FRP strip; 5 – Adhesive 1; 6 – Adhesive 2.

Fig. 1. Single-lap shear test of a: (a) mixed-adhesive bonded joint; and (b) simplified mixed-adhesive bonded joint.

(i) the thicknesses of the adherends remain unchanged;
(ii) the adherends have a linear elastic behaviour;
(iii) bonded interface is subjected only to mode II stresses (i.e. interfacial shear stresses);
(iv) bond stresses are uniform across the width of the CFRP composite.

2.2. Bond-slip model

Different bond-slip laws (τ_b-s) are assumed for two regions with different adhesives. In the case of brittle adhesives, bond-slip relationships with a triangular shape have been used [55] while trapezoidal shapes have been associated with ductile adhesives [41]. Nevertheless, Jiang et al. [54] used an exponential bond-slip relationship to approximate the local bond behaviour of joints with brittle and ductile behaviours. Despite being different from the one proposed by Jiang et al. [54], the exponential bond-slip relationship proposed by Dai et al. [53] was assumed in this work since it is easier to derivate or integrate and has fewer parameters to define. Hence, the determination of a closed-form solution that can describe the full debonding process of the joints is facilitated.

Unlike the piecewise functions obtained from the triangular or trapezoidal bond-slip relationships, exponential bond-slip relationships do not require the definition of several expressions to define all the states that the interface undergoes until failure [56]. The exponential bond-slip relationship considers an initial Elastic (E) stage, Softening (S) stage, and Debonding (D) stage. Mathematically, this exponential bond-slip relationship is defined as [53]:

$$\tau_b = 2B \cdot G_F \cdot \left(e^{-B \cdot s} - e^{-2B \cdot s}\right) \tag{1}$$

where B is the stiffness index of the joint experimentally defined from the strain-slip curve; and G_F is the fracture energy determined according to

$$G_F = \frac{E_r \cdot t_r \cdot \varepsilon_{rmax}^2}{2} \tag{2}$$

where E_r and t_r are the elastic modulus and thickness of the reinforcement, respectively; and ε_{rmax} is the maximum strain in the reinforcement obtained from the debonding test.

The maximum bond stress can be found by carrying out the first derivative of Eq. (1) with respect to s that when equated to zero, the slip corresponding to τ_{bmax} is:

$$s_{max} = \frac{\ln(2)}{B} \tag{3}$$

Introducing Eq. (3) into Eq. (1), the maximum bond stress predicted by the exponential bond-slip relationship is:

$$\tau_{bmax} = \frac{B \cdot G_F}{2} \tag{4}$$

To define the exponential bond-slip relationship defined in Eq. (1) to brittle and ductile adhesives the results reported by Jiang et al. [54] were considered. Fig. 2 compares the results obtained from Eq. (1) with those reported by Jiang et al. [54]. In this case, the brittle adhesive was identified as the epoxy resin Sikadur 30 and it was originally tested by Wang et al. [57], whereas the ductile adhesive was identified as being Araldite 420 and it was experimentally tested by Yu et al. [58]. As shown in Fig. 2, the exponential bond-slip relationship defined in Eq. (1) leads to similar results to the ones obtained by Jiang et al. [54], which validates its use in the present work. Thus, for the brittle adhesive, Eq. (1) is defined when $B = 32.044$ mm^{-1} and $G_F = 1.451$N/mm leading to $\tau_{bmax} = 23.24$ MPa and $s_{max} = 0.022$ mm. In the case of the ductile adhesive, Eq. (1) is defined when $B = 2.246$ mm^{-1} and $G_F = 16.065$N/mm leading to

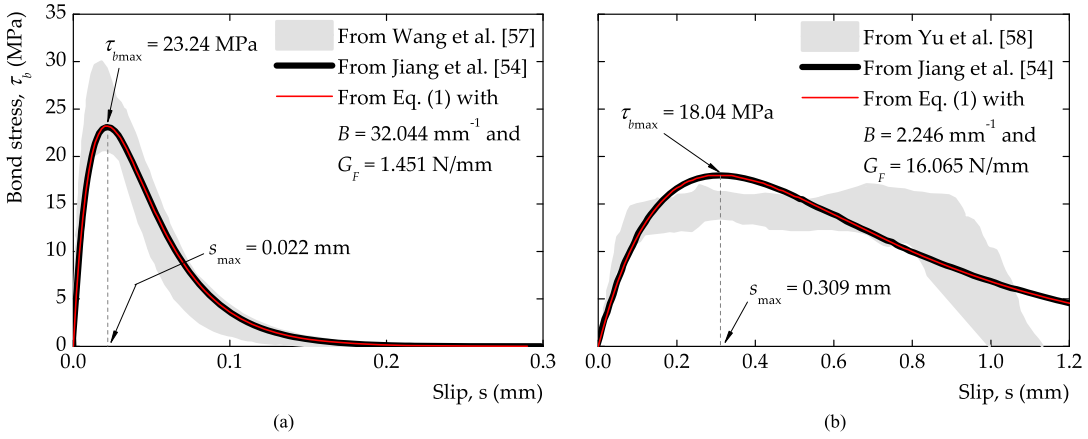

Fig. 2. Comparisons between exponential bond-slip relationships for the: (a) brittle adhesive; and (b) ductile adhesive.

$\tau_{bmax} = 18.04$ MPa and $s_{max} = 0.309$ mm.

2.3. Governing equation and proposed analytical solution

The definition of the governing equation of the debonding process can be made from the equilibrium of an infinitesimally small element of length dx, which based on the elastic behaviour of the adherends leads to the 2nd-order differential equation [39,43,59–63]:

$$\frac{d^2s}{dx^2} - \lambda \cdot \tau_b = 0 \tag{5}$$

where τ_b is the bond stress developed in the contact between the FRP composite and the substrate; s is the relative displacement (or slip) between adherends; x is the distance measured parallel to the bonded interface starting from the end of the bonded joint with adhesive 1 as shown in Fig. 1b; and λ is a constant defined according to:

$$\lambda = \frac{1}{E_r \cdot t_r} + \frac{b_r}{E_s \cdot A_s} \tag{6}$$

where E_r and E_s are the elastic moduli of the FRP composite (or reinforcement) and substrate, respectively; t_r and b_r are, the thickness and width of the FRP composite, respectively; and A_s is the cross-sectional area of the substrate. When the substrate is too stiff when compared with the FRP composite, i.e. when $E_s{\cdot}A_s \gg E_r{\cdot}t_r$, Eq. (6) is reduced to:

$$\lambda = \frac{1}{E_r \cdot t_r} \tag{7}$$

Depending on the bond-slip relationship that describes the local bond behaviour between adherends, Eq. (5) can be more or less difficult to solve. In some situations, Eq. (5) is only solved if a numerical strategy is implemented. As already mentioned, the exponential bond-slip model defined in Eq. (1) is quite versatile and when introduced into Eq. (5), leads to:

$$\frac{d^2s}{dx^2} - 2\lambda \cdot B \cdot G_F \cdot \left(e^{-B \cdot s} - e^{-2B \cdot s}\right) = 0 \tag{8}$$

To solve Eq. (8), the following relationship is used:

$$\frac{d^2s}{dx^2} = \frac{d}{dx}\left(\frac{ds}{dx}\right) = \frac{d}{ds}\left(\frac{ds}{dx}\right)\frac{ds}{dx} = \frac{1}{2} \cdot \frac{d}{ds}\left(\frac{ds}{dx}\right)^2 \tag{9}$$

Therefore, Eq. (8) can be rewritten as

$$\left(\frac{ds}{dx}\right)^2 = \int 4\lambda \cdot B \cdot G_F \cdot \left(e^{-B \cdot s} - e^{-2B \cdot s}\right) ds \tag{10}$$

Since

$$2B \cdot \left(e^{-B \cdot s} - e^{-2B \cdot s}\right) = \frac{d}{ds}\left(1 - e^{-B \cdot s}\right)^2 \tag{11}$$

Eq. (10) is rewritten as

$$\left(\frac{ds}{dx}\right)^2 = \int 2\lambda \cdot G_F \cdot \frac{d}{ds}\left(1 - e^{-B \cdot s}\right)^2 ds \tag{12}$$

The integration of Eq. (12) leads to:

$$\frac{ds}{dx} = \sqrt{D^2 \cdot \left(1 - e^{-B \cdot s}\right)^2 + C_1} \tag{13}$$

where C_1 is a constant; and D is a positive constant given by

$$D = \sqrt{2\lambda \cdot G_F} \tag{14}$$

To define the slips developed throughout the bond line of the joint, Eq. (13) is rewritten as

$$\frac{ds}{\sqrt{\left(1 - e^{-B \cdot s}\right)^2 + \left(\frac{\sqrt{|C_1|}}{D}\right)^2}} = D dx \tag{15}$$

which when integrated yields

$$\frac{D\cdot \operatorname{arsinh}\left(\frac{\left(D^2+C_1\right)\cdot e^{B\cdot s}-D^2}{\sqrt{|C_1|}\cdot D}\right)}{B\cdot\sqrt{|D^2+C_1|}}=D\cdot x+C_2 \tag{16}$$

where C_2 is a second constant obtained from the integration of Eq. (15).

Solving Eq. (16) with respect to s, the slips of the FRP-to-substrate throughout the bond line is

$$s(x)=\frac{1}{B}\cdot\ln\left[\frac{D^2+\sqrt{|C_1|}\cdot D\cdot\sinh\left(\frac{B\cdot(D\cdot x+C_2)\cdot\sqrt{|D^2+C_1|}}{D}\right)}{|D^2+C_1|}\right] \tag{17}$$

The definition of constant C_2 can be made by assuming that the slip developed at $x=0$ is $s=s_0$:

$$C_2=\frac{D\cdot \operatorname{arsinh}\left(\frac{\left(D^2+C_1\right)\cdot e^{B\cdot s_0}-D^2}{\sqrt{|C_1|}\cdot D}\right)}{B\cdot\sqrt{|D^2+C_1|}} \tag{18}$$

On the other hand, constant C_1 can be defined from the axial strains of the FRP composite developed at $x=0$. The FRP composite axial strains can be found through the following expression [38,46,64]:

$$\varepsilon_r=\frac{1}{1+r}\cdot\frac{ds}{dx} \tag{19}$$

where r is the ratio between the axial stiffness of the FRP composite and the axial stiffness of the substrate, respectively, i.e.

$$r=\frac{E_r\cdot A_r}{E_s\cdot A_s} \tag{20}$$

Therefore, when Eq. (13) is introduced into Eq. (19) the FRP composite axial strains at $x=0$ are defined according to:

$$\varepsilon_{r0}=\frac{1}{1+r}\cdot\sqrt{D\cdot\left(1-e^{-B\cdot s_0}\right)^2+C_1} \tag{21}$$

So, constant C_1 is defined as

$$C_1=\varepsilon_{r0}^2\cdot(1+r)^2-D^2\cdot\left(1-e^{-B\cdot s_0}\right)^2 \tag{22}$$

The FRP composite axial strains are obtained by using the following equation:

$$\varepsilon_r(x)=\frac{1}{1+r}\cdot\frac{\sqrt{|C_1+D^2|}\cdot\cosh\left(\frac{B\cdot(D\cdot x+C_2)\cdot\sqrt{|C_1+D^2|}}{D}\right)}{\sinh\left(\frac{B\cdot(D\cdot x+C_2)\cdot\sqrt{|C_1+D^2|}}{D}\right)+\frac{D}{\sqrt{|C_1|}}} \tag{23}$$

To define the strains developed in the substrate, the following equation can be used [38,46,64]:

$$\varepsilon_s=-\frac{1}{1+\frac{1}{r}}\cdot\frac{ds}{dx} \tag{24}$$

So, the strains in the substrate are defined as

$$\varepsilon_s(x)=-\frac{1}{1+\frac{1}{r}}\cdot\frac{\sqrt{|C_1+D^2|}\cdot\cosh\left(\frac{B\cdot(D\cdot x+C_2)\cdot\sqrt{|C_1+D^2|}}{D}\right)}{\sinh\left(\frac{B\cdot(D\cdot x+C_2)\cdot\sqrt{|C_1+D^2|}}{D}\right)+\frac{D}{\sqrt{|C_1|}}} \tag{25}$$

Finally, the definition of the bond shear stresses developed throughout the bond line of the joint is obtained by introducing Eq. (17) into Eq. (1), which yields:

$$\tau_b(x) = 2B \cdot G_F \cdot \frac{\dfrac{D}{\sqrt{|C_1|}} + \dfrac{\sqrt{|C_1|}}{D}}{\dfrac{D}{\sqrt{|C_1|}} + \sinh\left(B \cdot (D \cdot x + C_2) \cdot \sqrt{\left|1 + \dfrac{C_1}{D^2}\right|}\right)} \times \left(1 - \frac{\dfrac{D}{\sqrt{|C_1|}} + \dfrac{\sqrt{|C_1|}}{D}}{\dfrac{D}{\sqrt{|C_1|}} + \sinh\left(B \cdot (D \cdot x + C_2) \cdot \sqrt{\left|1 + \dfrac{C_1}{D^2}\right|}\right)}\right) \tag{26}$$

3. Validation of the analytical solution

To validate the analytical solution proposed in the previous section, different bonded joints with different configurations are idealized. For simplicity, a few specimens with short or long bonded lengths with brittle or ductile adhesives were selected. Thus, the bonded joints with only one adhesive with different bonded lengths (L_b) are used for reference purposes. A combination of both adhesive types with the bonded lengths of the reference specimens are also idealized so a series of mixed-adhesive joints would be analyzed and allowed the validation of the analytical solution. Since an enormous number of materials and dimensions could be considered for the bonded joints, a unidirectional CFRP composite and a steel substrate are selected. Also, the mechanical properties and dimensions are fixed and are reported later. All idealized specimens are then simulated with a commercial finite element software package [65]. Therefore, a brief description of the numerical modelling carried out in this work is presented.

It should be noted also that the analytical model can be used by assuming a spring with a residual stiffness with marginal (or none) influence on the debonding process of the CFRP-to-steel joints. Therefore, for the analytical simulation of the CFRP-to-steel joints with mixed adhesives, the stiffness of the nonlinear spring can be obtained from the first half of the joint closed to the CFRP unloaded end (see Fig. 1), which corresponds to a reference specimen, i.e., with the load-slip relationship obtained from the specimens with a single adhesive. Only then, the mixed-adhesive joints are simulated, as shown in Fig. 1b, with the analytical model.

The quantification of the deviations between the results obtained from the proposed analytical solution and those obtained from the FEM is made using the Integral Absolute Error (IAE). This parameter is widely used by many researchers for model assessment [64,66,67]. The IAE is calculated according to:

$$IAE = \sum_{s=1}^{n} \frac{\left|d_{s,PAS} - d_{s,FEM}\right|}{\sum_{s=1}^{n} d_{s,FEM}} \tag{27}$$

Table 1
ID of the bonded joints.

ID	Bonded length, L_b (mm)	Adhesives
CS-L50S	50	Sikadur 30
CS-L100S	100	
CS-L150S	150	
CS-L200S	200	
CS-L300S	300	
CS-L50A	50	Araldite 420
CS-L100A	100	
CS-L150A	150	
CS-L200A	200	
CS-L300A	300	
CS-L50S-L50A	50 + 50	Sikadur 30 + Araldite 420
CS-L50S-L100A	50 + 100	
CS-L100S-L50A	100 + 50	
CS-L100S-L100A	100 + 100	
CS-L50S-L150A	50 + 150	
CS-L150S-L50A	150 + 50	
CS-L150S-L150A	150 + 150	
CS-L100S-L200A	100 + 200	
CS-L200S-L100A	200 + 100	
CS-L50A-L50S	50 + 50	Araldite 420 + Sikadur 30
CS-L50A-L100S	50 + 100	
CS-L100A-L50S	100 + 50	
CS-L100A-L100S	100 + 100	
CS-L50A-L150S	50 + 150	
CS-L150A-L50S	150 + 50	
CS-L150A-L150S	150 + 150	
CS-L100A-L200S	100 + 200	
CS-L200A-L100S	200 + 100	

where $d_{s,PAS}$ and $d_{s,FEM}$ correspond to the data obtained from the proposed analytical solution and those calculated from the FEM, respectively, at the same slip; and n corresponds to the number of measurements carried out during the simulations of the debonding process. IAE values equal to or lower than 10% may indicate that the analytical solution can replicate the numerical simulations with sufficient accuracy so it can be considered as being validated.

3.1. Characteristics of the bonded joints

The specimens considered for the FEM as well as analytical predictions were CFRP-to-steel single lap shear pull tests as shown in Fig. 1. Since the effective bond length of the joints is unknown, different bonded lengths (L_b) of 50, 100, 150, 200, and 300 mm were selected for all the bond joint adhesive configurations, so the influence of the bond length could be investigated.

The same CFRP composite used by the author in another work [68] was considered. In the direction of the carbon fibres, the elastic modulus of the CFRP is 159 GPa, with a tensile strength of 1,565 MPa, and a corresponding rupture strain approximately equal to 1.0%. Supplied by a local S&P seller, the CFRP strip has a thickness of 1.4 mm and a width of 10 mm. As a substrate, a hollowed rectangular steel profile with an elastic modulus of 200 GPa and yielding strain of 0.2% is considered. The cross-sectional area of the steel profile is 150 mm of side and a steel thickness of 7 mm. Thus, the axial stiffness ratio defined in Eq. (20) of the specimens is approximately 0.01.

To bond the CFRP composite to the steel profile, the already mentioned epoxy resins Sikadur 30 and Araldite 420 were considered which, according to Jiang et al. [54], led to two different local bond adherences that can be approximated by an exponential bond-slip relationship whose parameters were defined in subsection 2.2.

3.2. Identification of the bonded joints

The different bonded joint configurations analyzed in this work are listed in Table 1. A total of 28 configurations were analyzed. To facilitate the readership of the text and identification of each specimen, a particular nomenclature was created in which the materials of the adherends are identified as well as the bonded length of the specimens and the adhesive types. For instance, specimen CS-L50S-L150A intends to identify the specimen where a CFRP-to-steel (CS) bonded joint in which the left hand of the joint has a bond line of 50 mm with Sikadur 30 epoxy resin (brittle adhesive) while the right hand of the joint has a bond line of 150 mm with Araldite 420 epoxy resin (ductile adhesive).

3.3. Numerical modelling

Although various FEM have been used to model the bond behaviour between a CFRP composite externally bonded to a steel substrate, e.g., [69–73], all the finite element models were simulated as 2D specimens in ATENA [65]. This software has already proven to be quite accurate in the prediction of a varied number of debonding problems, e.g. [46,47,74,75]. For simplicity, a 2D version of ATENA software [65] was used rather than its 3D version so the number of unknowns and nonlinear equations to be solved by the Newton-Raphson method could be reduced significantly. Since the analytical solution is a 1D problem, it is also expected that the 2D version of ATENA [65] could be as close to the analytical solution as possible. Also, by reducing significantly the number of finite elements the time taken to process a single simulation can be reduced. In other studies by the authors, this strategy was conducted with good results without losing the precision [46,47].

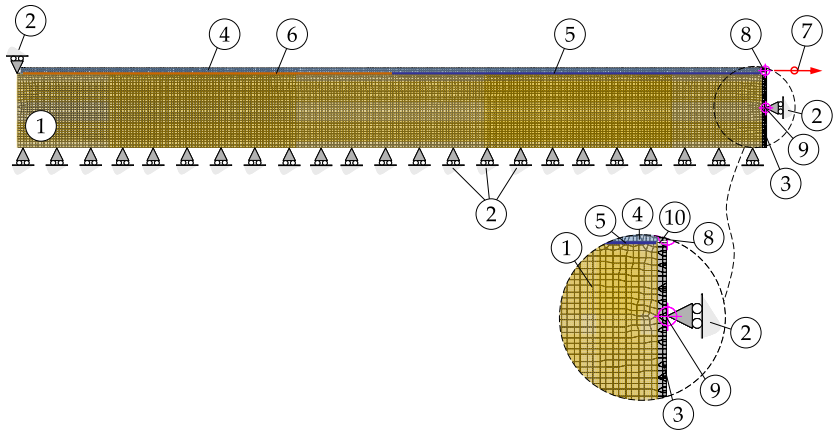

Key: 1 – Steel substrate; 2 – Roller support; 3 – Reaction rigid material; 4 – CFRP composite; 5 – Adhesive 1; 6 – Adhesive 2; 7 – Loading increment; 8 – Displacement control; 9 – Reaction control; 10 – Interface with no contact.

Fig. 3. Example of the finite element mesh of the mixed-adhesive CFRP-to-steel joints CS-L50S-L150A or CS-L50A-L150S.

The bonded interface was modelled using a coupled CZM approach, which was based on the Mohr-Coulomb failure criterion with tension cut-off. Since in single-lap shear pull tests, the bonded interface is subjected to non-negligible peeling stresses, coupling between mode I and mode II has no real effect, thus the friction angle which is required for defining the Mohr-Coulomb criterion has a negligible effect on the results, thus ignored.

Loading was applied as an axial displacement (at a displacement rate of 0.002 mm per step) on the loaded end of the CFRP laminate (see Fig. 3). During the simulations of the mixed-adhesive joints, three monitoring points were considered. The first two monitoring points were placed at the CFRP-loaded end. One controlled the loads transmitted to the CFRP composite and the other one controlled the displacements (see 8 in Fig. 3). The third monitoring point controlled the reaction of the steel plate at its midpoint (see 9 in Fig. 3), which, from an equilibrium point of view, should be equal to the loads transmitted to the CFRP composite. Otherwise, the simulation has some errors and, therefore, it should not be considered. The failure of the specimens was reached in all specimens regardless of the number of steps needed to carry out the simulations.

Close to the contact between adherends a discretized mesh of 0.4 to 0.5 mm quadrilateral finite elements with smooth element shapes was considered. The total number of finite elements in each specimen varied due to their different bonded lengths. Therefore, in the models with the shortest bonded length such as CS-L50S and CS-L50A a total of 7275 finite elements were used. This number of finite elements increases to 12,395 in the models with a total bonded length of 300 mm such as e.g., CS-L300A, CS-L150S-L150A or CS-L100S-L200A. The numerical simulations were carried out in a laptop computer with an Intel Core i7-7700HQ at 2.80 GHz with 16 GB of 2400 MHz RAM. The simulations took approximately 20 min (in the specimens with the lowest number of finite elements) to 60 min (in the specimens with the highest number of finite elements).

3.4. Load-slip curves

The load-slip curves obtained from the analytical solution are compared with those obtained from the FEM and the results are presented and discussed in this subsection. It should be mentioned that the strain-slip (or load-slip) curves obtained from the analytical solution followed two paths. One followed Eqs. (17) and (23) and the other also calculates the slips according to Eq. (17) but the loads transmitted to the FRP composite are calculated by considering the equilibrium of the FRP composite, i.e.:

$$F = \int_0^{L_b} \tau(x)dA + F_0 = b_r \cdot \int_0^{L_b} \tau(x)dx + F_0 \tag{28}$$

Table 2
Main results obtained from the analytical and FEM.

ID	Analytical solution		FEM		Deviation (%)	
	Max. load, F_{max} (kN) [(1) | (2)]	Disp. at F_{max} (mm) [(1) | (2)]	Max. load, F_{max} (kN)	Displ. at F_{max} (mm)	Max. load [(1) | (2)]	Max. displ. [(1) | (2)]
CS-L50S	7.77 | 7.15	0.124 | 0.093	7.37	0.102	5.4 | −3.0	21.6 | −8.8
CS-L100S	7.99 | 7.94	0.246 | 0.180	7.72	0.222	3.5 | 2.9	10.8 | −18.9
CS-L150S	7.99 | 7.99	0.367 | 0.269	7.75	0.512	3.1 | 3.1	−28.3 | −47.5
CS-L200S	7.99 | 7.99	0.488 | 0.360	7.75	0.512	3.1 | 3.1	−4.7 | −29.7
CS-L300S	7.99 | 7.99	0.730 | 0.542	7.76	0.848	3.0 | 3.0	−13.9 | −36.1
CS-L50A	8.64 | 8.90	0.544 | 0.511	8.97	0.382	−3.7 | −0.8	42.4 | 33.8
CS-L100A	20.99 | 15.83	0.851 | 0.708	17.03	0.592	23.3 | −7.0	43.8 | 19.6
CS-L150A	24.22 | 20.49	1.236 | 0.978	22.31	0.944	8.6 | −8.2	30.9 | 3.6
CS-L200A	25.64 | 23.24	1.647 | 1.245	24.94	1.272	2.8 | −7.0	29.5 | −2.1
CS-L300A	26.45 | 25.66	2.465 | 1.830	26.46	2.224	0.0 | −3.0	10.8 | −17.7
CS-L50S-L50A	16.08 | 16.08	0.403 | 0.403	15.61	0.364	3.0 | 3.0	10.7 | 10.7
CS-L50S-L100A	22.91 | 22.91	0.838 | 0.838	22.74	0.796	0.8 | 0.8	5.3 | 5.3
CS-L100S-L50A	22.29 | 16.69	0.578 | 0.491	16.48	0.468	35.3 | 1.3	23.7 | 4.9
CS-L100S-L100A	23.07 | 23.08	0.860 | 0.860	22.88	0.826	0.8 | 0.9	4.1 | 4.1
CS-L50S-L150A	25.88 | 25.89	1.344 | 1.344	25.76	1.300	0.5 | 0.5	3.4 | 3.4
CS-L150S-L50A	17.40 | 16.69	0.578 | 0.494	16.49	0.480	5.5 | 1.2	20.4 | 2.9
CS-L150S-L150A	25.96 | 25.97	1.358 | 1.358	25.78	1.310	0.7 | 0.7	3.7 | 3.7
CS-L100S-L200A	26.91 | 26.92	1.919 | 1.919	26.74	1.858	0.6 | 0.6	3.3 | 3.3
CS-L200S-L100A	23.07 | 23.08	0.861 | 0.861	22.88	0.826	0.8 | 0.8	4.2 | 4.2
CS-L50A-L50S	8.67 | 8.67	0.675 | 0.675	8.97	0.584	−3.3 | −3.3	15.6 | 15.6
CS-L50A-L100S	8.67 | 8.67	0.872 | 0.872	8.98	0.786	−3.3 | −3.3	10.9 | 10.9
CS-L100A-L50S	20.99 | 20.99	1.327 | 1.327	17.03	0.968	20.3 | 20.3	37.1 | 37.1
CS-L100A-L100S	20.99 | 20.99	1.803 | 1.803	17.03	1.348	20.3 | 20.3	33.8 | 33.8
CS-L50A-L150S	8.67 | 8.67	1.070 | 1.070	8.98	0.992	−3.3 | −3.3	7.9 | 7.9
CS-L150A-L50S	24.22 | 24.22	1.784 | 1.784	22.31	1.446	8.6 | 8.6	23.4 | 23.4
CS-L150A-L150S	24.22 | 24.22	2.884 | 2.884	22.31	2.434	8.6 | 8.6	18.5 | 18.5
CS-L100A-L200S	20.99 | 20.99	2.756 | 2.756	17.04	2.118	1.4 | 1.4	30.1 | 30.1
CS-L200A-L100S	25.64 | 25.64	2.811 | 2.811	24.94	2.464	2.8 | 2.8	14.1 | 14.1

(1) Results considering Eqs. (17) and (23);
(2) Results considering Eqs. (17) and (28).

where L_b here represents the length of the bonded region with adhesive 1, i.e. the part of the bonded joint shown in Fig. 1b; and F_0 is the force in the nonlinear spring. By dividing the bond length L_b into n number of segments, the integral (I) in Eq. (28), can be approximated as:

$$I = \frac{b_r}{2} \cdot \sum_{i=0}^{i=n} (\tau_{i+1} + \tau_i) \cdot (x_{i+1} - x_i) \tag{29}$$

where x_{i+1} and x_i are the distance to the discretized points i+1 and i, respectively; and τ_{i+1} and τ_i are the bond stresses developed at discretized points i+1 and i, respectively.

As already mentioned, the specimens with a single adhesive are used as reference specimens. Therefore, the results of mixed-adhesive specimens are compared with the reference specimens of the same total bond length (L_t) to investigate the effect of the use of mixed-adhesives. For easy comparison, Table 2 summarizes the key results obtained from the analytical solution and the FEM. The deviations shown in Table 2 are determined according to:

$$D = \frac{r_{analytical} - r_{numerical}}{r_{numerical}} \times 100\% \tag{30}$$

where $r_{analytical}$ and $r_{numerical}$ correspond to the results (i.e. maximum load and displacement at maximum load) obtained from the proposed analytical solution and those obtained from the FEM, respectively.

3.5. Single-adhesive joints

Fig. 4 shows the load-slip curves of the single-adhesive bonded joints obtained from the analytical solution and the FEM. The load-slip curves are organized according to the adhesive type, i.e. brittle in Fig. 4a and ductile in Fig. 4b. The results show that the use of the ductile adhesive leads to the highest load capacities of the single-adhesive joints. However, when the bonded length is short (i.e. 50 mm) the difference in the load capacity of bonded joints with two different adhesives was small, i.e. approximately 8.0 kN for adhesive type S and 9.0 kN for adhesive type A. As the bonded length increases, the load capacities of the specimens with the ductile adhesive tend to increase whereas the single-adhesive joints with the brittle adhesive remained unchanged. This means that the effective bond length of the single-adhesive joints with the brittle adhesive has an effective bond length of approximately 50 mm. In the case of the specimens with the ductile adhesive, the effective bond length may stay approximately between 200 mm and 300 mm since the maximum loads transmitted to the CFRP composite remained almost unchanged in those two cases. These differences between the brittle and ductile adhesive can be explained by the interfacial fracture work per unit area associated with each bond-slip relationship, where in the case of adhesive type A showed a lower initial stiffness and a much higher slip at debonding than that for type S adhesive.

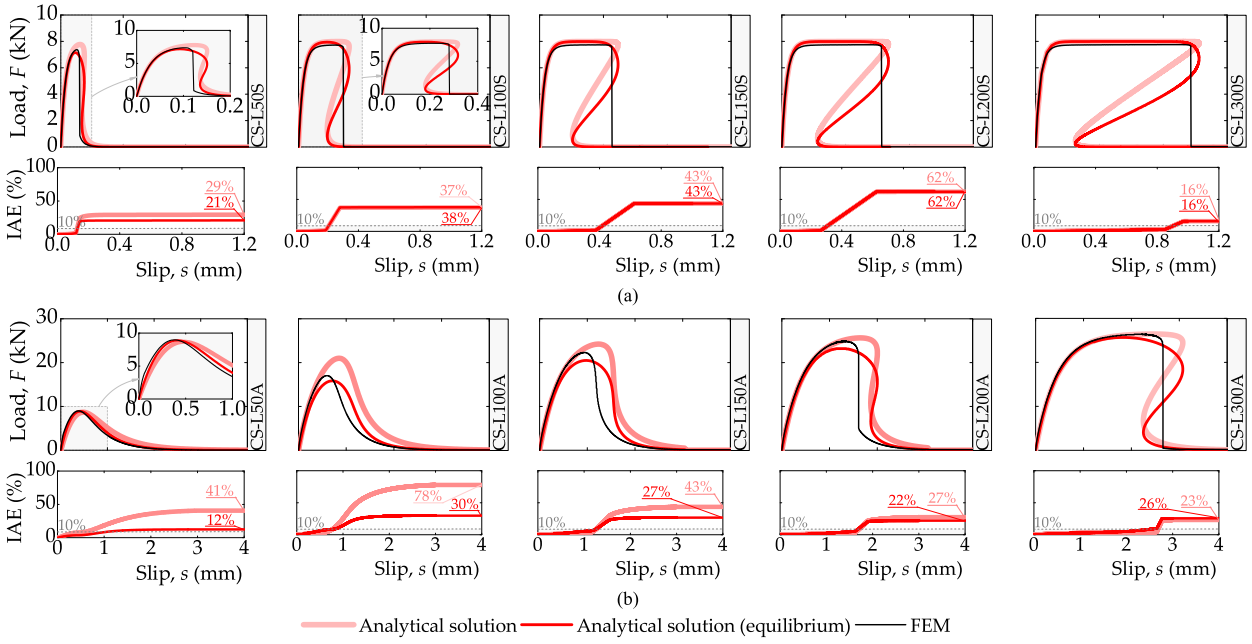

Fig. 4. Accuracy of the load-slip curves obtained by the proposed analytical approach with the FEM of the single-adhesive joints with a: (a) brittle adhesive; and (b) ductile adhesive.

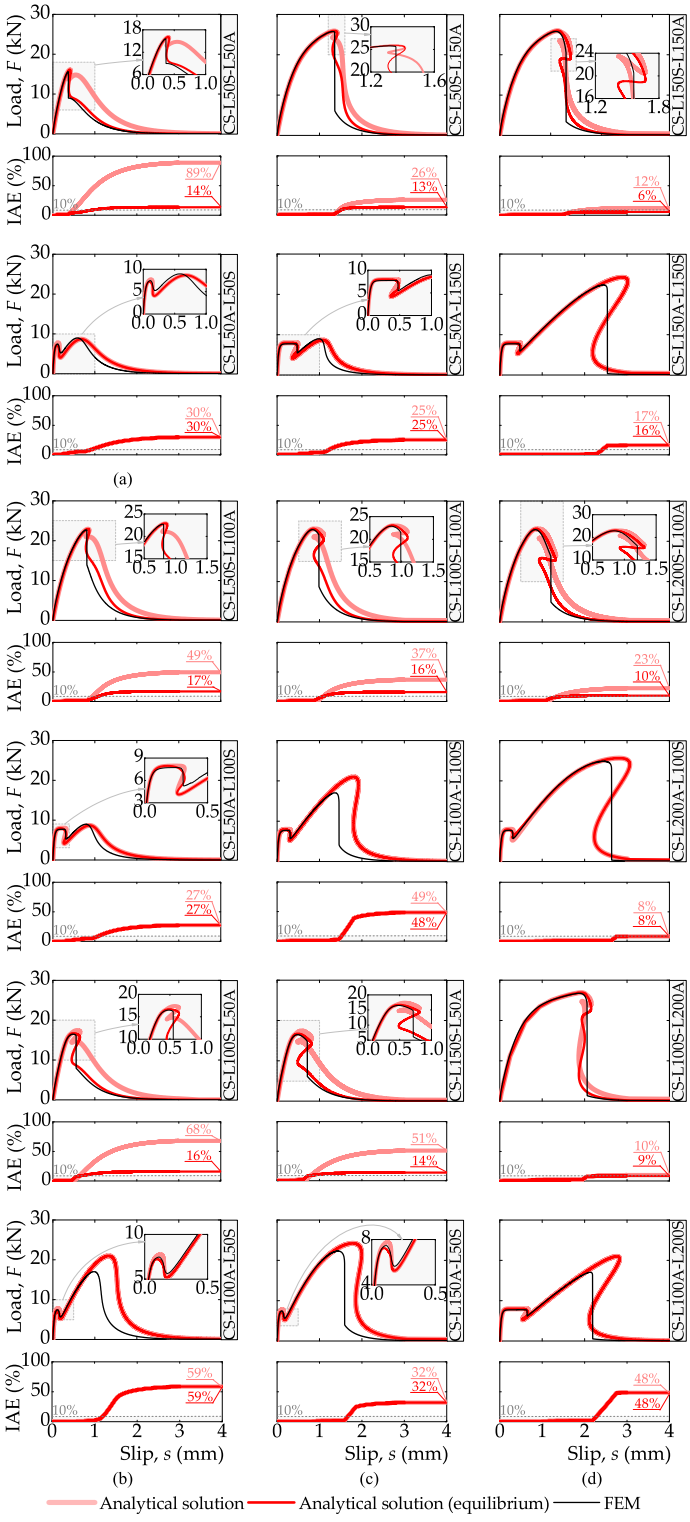

Fig. 5. Accuracy of the load-slip curves obtained by the proposed analytical approach with the FEM of the mixed-adhesive joints with a total length of: (a) $L_t = 100$ mm; (b) $L_t = 150$ mm; (c) $L_t = 200$ mm; and (d) $L_t = 300$ mm.

This increased effective bond length for adhesive type A compared to adhesive type S was also reported by Fernando et al. [41] and Yu et al. [58].

Moreover, for long bonded lengths, after the maximum load is reached, the loads tend to decrease. However, this load decrease is followed by a slip decrease, which is known as a snapback phenomenon. This snapback phenomenon can occur in the single-adhesive joints with a brittle adhesive with 100 mm, 150 mm, 200 mm and 300 mm as well as in the specimens with a ductile adhesive with 200 mm and 300 mm. Hence, this corroborates with the identification of the effective bond length of the joints. After a certain point, the slips tend to increase with the load decrease and for high slip values the load transmitted to the CFRP composite is zero and the joint is fully debonded.

Comparing both load-slip curves obtained by the analytical model, it can be seen that the main differences occur when the loads tend to decrease, i.e. after the maximum load capacity of the joint is reached. In both cases, the maximum loads reached in the specimens with the brittle adhesive are slightly higher than that obtained from the FEM. However, looking at the specimens with the ductile adhesive, it can be seen that from the equilibrium equation in (28) the maximum loads transmitted to the CFRP composite are lower than those obtained from the FEM. The use of Eqs. (17) and (19) led to the highest maximum loads transmitted to the CFRP composite, particularly in specimens CS-L100A and CS-L150A.

The IAE values are all lower than 10% until the maximum load is predicted by the FEM. After that point, the IAE values tended to increase. In some cases, values higher than 50% were determined (CS-L200S and CS-L100A). Nevertheless, those results may not be meaningful since they correspond to the significant differences between the loads at the same slip where they are hard or even impossible to determine experimentally. However, these differences between the use of Eqs. (17) and (19) with the use of equilibrium equation in (28) may lead to some differences when used to define the mixed-adhesive joints.

3.6. Mixed-adhesive joints

To simulate the mixed adhesive joints, the single-adhesive joints were considered first and then the load-slip curves were obtained from Eqs. (17) and (19) were used to simulate the nonlinear springs. Fig. 5 compares the final load-slip curves of the mixed-adhesive joints obtained from the analytical solution with those obtained from the FEM. The analytical predictions agreed well with the FEM results. The mixed-adhesive bonded joints showed significantly different load-slip behaviours to those of single-adhesive bonded joints and the length ratio between adhesive types S and A had a significant influence on the load-slip behaviour.

All the combinations considered in this work led to different load-slip curves. Thus, in the case with a total length (L_t) of only 100 mm it can be seen that when the ductile adhesive is used at the CFRP-loaded end (i.e. at the right-hand side of the mixed-adhesive joint), the load capacity of the mixed-adhesive joints increases (see Fig. 5a). This can be explained by its influence from the beginning of the debonding process until the failure of the joint, which does not occur when the ductile adhesive is used on the left-hand side of the joint.

The same seems to occur when the total bonded length increases to $L_t = 100$ mm. The highest load capacity was reached in specimen CS-L50S-L100A (22.91 kN). Even when the corresponding bonded length of the ductile adhesive is 50 mm specimen CS-L100S-L50A the maximum load was 22.29 kN. It can be seen also that in specimens CS-L50A-L100S and CS-L100A-L50S, a plateau or a first peak load can be seen, respectively. This means that the region with the fragile adhesive has debonded before the ductile adhesive has mobilized. Therefore, the ductile adhesive is responsible for the appearance of a second peak in the load-slip curve, which is higher in the case of a longer ductile bonded length.

Similar characteristics can be seen in the other specimens with total bonded lengths of 200 mm and 300 mm (see Fig. 5c and 5d). However, with higher bonded lengths, the maximum loads increase. It should be noticed also that two snapbacks can be seen when the brittle adhesive is used close to the CFRP loaded end. The first one corresponds to the complete debonding of the brittle adhesive whereas the second corresponds to the full debonding of the joint. However, unlike the first snapback where the joints were able to stand the loads, the second snapback led the load-slip curve to zero load.

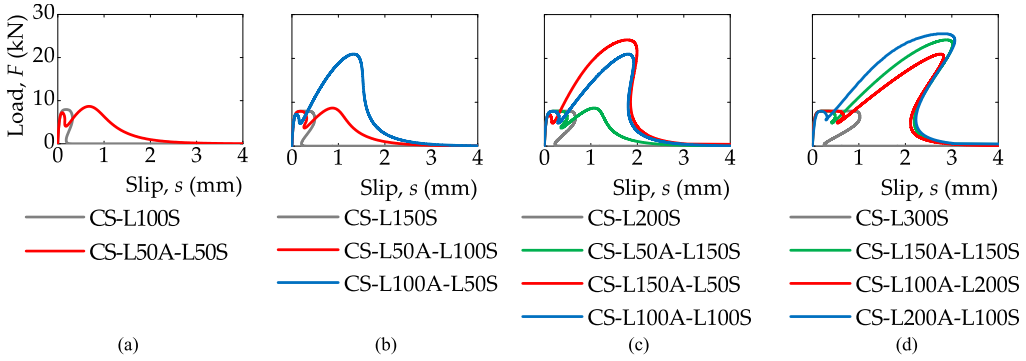

Fig. 6. Comparison of the load-slip curves obtained from the specimens with the brittle adhesive used close to the CFRP loaded end and with the same total length of: (a) $L_t = 100$ mm; (b) $L_t = 150$ mm; (c) $L_t = 200$ mm; and (d) $L_t = 300$ mm.

The analytical results are in fair agreement with those obtained from the FEM. However, using the equilibrium condition in (28) the results are more accurate with the FEM in the last branch of the load-slip curves, i.e. before full debonding of the joints. These differences can be attributed to some differences already identified in the single-adhesive joints. Nevertheless, until the first and unique snapback phenomenon (in the specimens where the ductile adhesive is used at the CFRP loaded end, e.g. CS-L50S-L50A, CS-L50S-L150A or CS-L100S-L200A) the IAE values are all lower than 10%. The same can be seen in the specimens with a second snapback phenomenon, i.e. in the specimens where the brittle adhesive is used at the CFRP-loaded end, where IAE values lower than 10% were determined until that point.

3.7. Bonded joints with the same total bonded length

As already shown, the use of the ductile adhesive close to the CFRP-loaded end leads to higher load capacities of the bonded joints. However, to better understand the influence of the ductile adhesive on the brittle adhesive and vice-versa, Figs. 6 and 7 show the load-slip curves obtained from the analytical solution where the equilibrium Eq. (28) was used. Fig. 6 shows that the use of ductile adhesive as an additional anchorage can significantly increase the load capacity and ductility of the joint. So, in the case of strengthening an existing structure with a brittle adhesive, the use of a ductile adhesive as an additional anchorage can be a good option as long as its length is larger than the effective bond length. Otherwise, the load capacity of the joints is barely increased (see Fig. 6a).

On the other hand, i.e. when an existing structure is externally bonded with a ductile adhesive, the use of a brittle adhesive as an additional anchorage almost leads to marginal maximum load increases. Furthermore, the maximum loads increase when the length of the anchorage with brittle adhesive is the shortest (see Fig. 7). However, for the same total bonded length, this option shows a decrease in the ductility (in displacement) of the joint, i.e. the ductility of the single joint with the ductile adhesive decreases when the additional anchorage with a brittle adhesive is considered.

Fig. 8 compares, for the same total bonded length, the influence of the positioning of the adhesive types in the mixed-adhesive joints. The results show that the load-slip curves of the mixed-adhesive joints initially follow the same path as the load-slip curve of the single-adhesive joints with the same adhesive that is placed on the right-hand side, i.e. at the CFRP loaded end. For instance, CS-L150A-L150S and CS-L300S exhibit a similar initial branch of their load-slip curve, whereas specimen CS-L150S-L150A has an initial load-slip curve similar to specimen CS-L300A. Except for the final branch of the load-slip curves of the specimens where the ductile adhesive is placed at the right-hand side (e.g. specimens CS-L100S-L100A or CS-L150S-L150A), a similar initial path to its homologous single-adhesive joint can be observed.

3.8. Bond stress distributions

To analyze the bond stresses developed throughout the bond line and allow the understanding of the debonding process of the mixed-adhesive joints, different slips at the CFRP loaded end were selected: 0.060 mm, 0.120 mm, 0.240 mm, 0.480 mm, 0.960 mm, 1.920 mm, 3.840 mm. The results are also compared with the bonded stresses developed in the single-adhesive joints. For simplicity, the bond stresses of the longest bonded lengths are presented, i.e. with $L_t = 300$ mm. In the case of the mixed-adhesive joints, the same bonded length using a brittle and ductile adhesive is reported. Therefore, the results obtained from reference specimens CS-L300S and CS-L300A as well as specimens CS-L150S-L150A and CS-L150A-L150S are considered.

The results are shown in Fig. 9. In the four shown cases, the debonding processes are carried out from the right-hand side to the left-hand side. From the single-adhesive joints, it can be seen that using the adhesive type S (i.e. in specimen CS-L300S in Fig. 9a) the bond stresses develop within a shorter interval than that observed from specimen CS-L300A (see Fig. 9b), which agrees with the observed shorter effective bond length of the adhesive type S bonded joints. Like in the single-adhesive joints, e.g. [41–43,56,70,76,77], the bond stresses developed in the mixed adhesive joints migrate towards the unpulled end with the increase of the slips.

From the mixed-adhesive joints, it can be seen that the bond stresses developed in both joints show a discontinuity at 150 mm due to the change of the bond-slip relationship at that point. Compared with specimen CS-L150A-L150S in Fig. 9c, the bond stresses developed in specimen CS-L150S-L150A (see Fig. 9c) mobilise the brittle region at a lower slip magnitude. Consequently, the stiffness

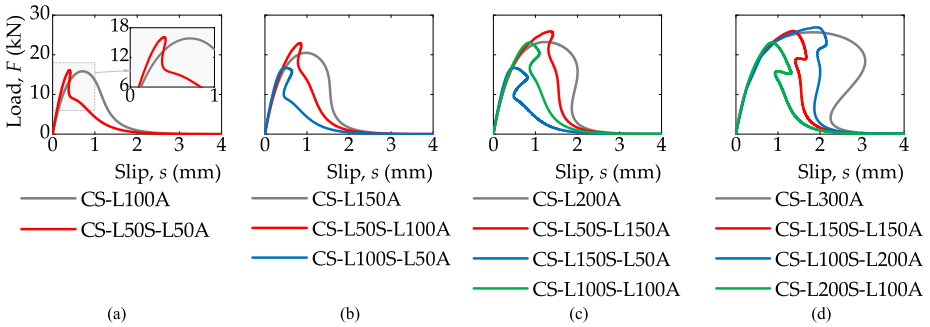

Fig. 7. Comparison of the load-slip curves obtained from the specimens with the ductile adhesive used close to the CFRP loaded end and with the same total length of: (a) $L_t = 100$ mm; (b) $L_t = 150$ mm; (c) $L_t = 200$ mm; and (d) $L_t = 300$ mm.

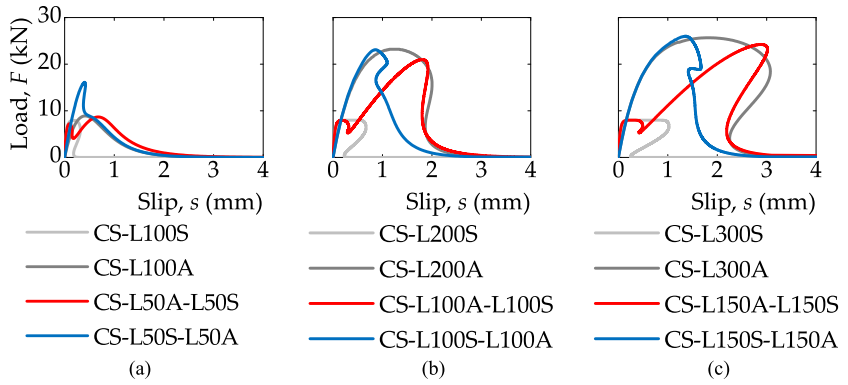

Fig. 8. Influence of the position of the adhesive type on the load-slip curve of the mixed-adhesive joint: (a) $L_t = 100$ mm; (b) $L_t = 200$ mm; and (c) $L_t = 300$ mm.

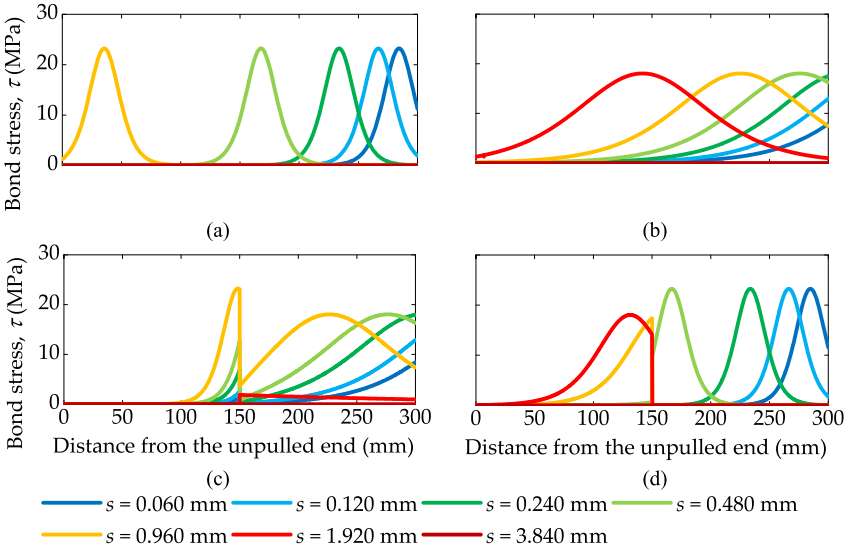

Fig. 9. Bond stress distributions of specimens: (a) CS-L300S; (b) CS-L300A; (c) CS-L150S-150A; and (d) CS-L150A-L150S.

of specimen CS-L150S-L150A is higher than that of specimen CS-L150-L150A (see also Fig. 6d and 7d). Thus, even before the ductile region of the specimen, CS-L150S-L150A has completely debonded the brittle region to develop bond stresses. For this reason, the maximum load transmitted to the CFRP composite is slightly increased (see also Fig. 7d). On the other hand, at the lowest slip magnitudes, the bond stresses developed in the brittle region of specimen CS-L150A-L150S are concentrated in this region and only after the debonding initiation, the ductile region is deformed. This can facilitate the interpretation of the load-slip curve obtained in this mixed-adhesive joint shown in Fig. 8c as well as the other similar load-slip curves shown, e.g., in Fig. 6 and Fig. 8.

3.9. Axial strain distributions

Following the same rationale of the previous subsection, this subsection describes the strains developed throughout the bonded length of specimens CS-L300S, CS-L300A, CS-L150S-L150A, and CS-L150A-L150S developed in the CFRP composite as well as in the steel substrate. Thus, the CFRP and steel strains developed in the previously mentioned specimens shown in Fig. 10 correspond to the same slip magnitudes assumed in the previous subsection, i.e., 0.060 mm, 0.120 mm, 0.240 mm, 0.480 mm, 0.960 mm, and 1.920 mm. Since for $s = 3.840$ mm the CFRP composite has completely debonded from the substrate, the strains developed in the specimens for this particular slip are not shown.

Fig. 10 compares the axial strain distributions, i.e., parallel with the bond line of the specimens, obtained by the analytical model with the numerical simulations. From an overall overview of this figure, it can be identified where the maximum strains develop, i.e., in the CFRP composite rather than the steel substrate where the strains are marginal. Particularly, the maximum CFRP strains develop at the CFRP-loaded end and tend to zero towards the CFRP-unloaded end. In the case of the reference specimen CS-L300A the transition from the highest CFRP strains to the lowest strains is smoother than in reference specimen CS-L300S as can be seen from the longest

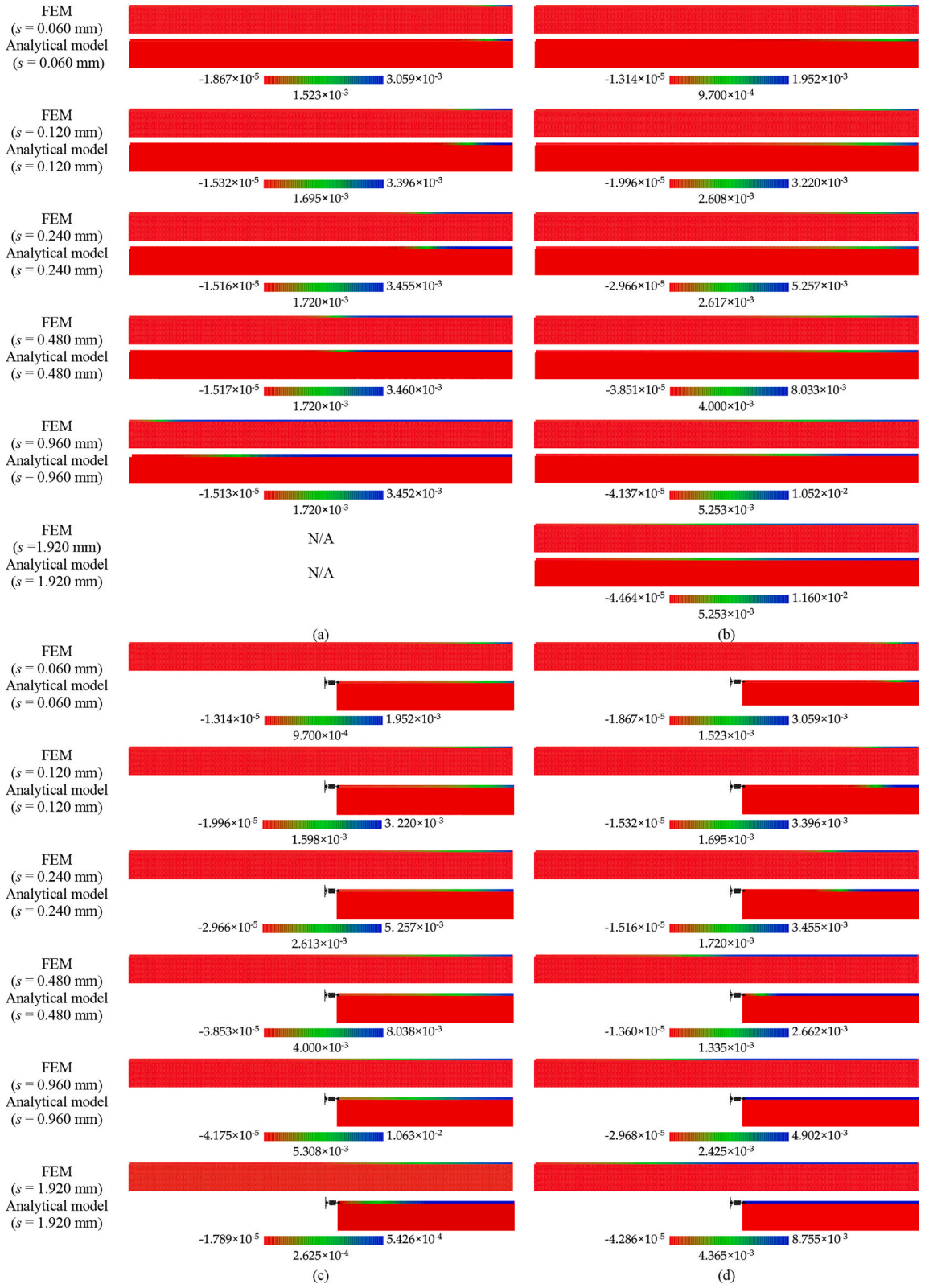

Fig. 10. Axial strain distributions in the specimens: (a) CS-L300S; (b) CS-L300A; (c) CS-L150S-150A; and (d) CS-L150A-L150S.

lengths under green colour in Fig. 10b.

It should be noted also that the analytical results corresponding to specimens CS-L150S-150A (in Fig. 10c) and CS-L150A-150S (in Fig. 10d) are shown for only one-half of the total length of the specimen since the other half is replaced by the nonlinear spring with the same load-slip relationship of the specimen with the same bonded length, i.e., with 150 mm, and adhesive type. For instance, in specimen CS-L150A-L150S (see Fig. 10d), when the slip at the CFRP-loaded end is 0.960 mm or 1.920 mm, the CFRP strains reach a maximum value (in blue colour) that covers the full length of the analytical model, which means this length is fully debonded. This can be confirmed from Fig. 9d where the bond stresses developed in this part of the specimen are zero for those two same slips. Nevertheless, it can be observed that the CFRP strain distributions obtained by the analytical model can fairly predict the numerical simulations.

4. Comparisons with other studies

To the best author's knowledge, no other studies are available in the literature so the proposed analytical solution could be compared. Nevertheless, some bonded joints using a single-adhesive were selected from the literature and then modified according to the idea of a mixed-adhesive joint. The results found in the literature are, therefore, used as reference and their corresponding mixed-adhesive joints are useful to investigate their new debonding process and load capacities. Hence, three studies were considered in the literature [78–80], in which, the bond behaviour of FRP-to-substrate joints with a single adhesive was experimentally and numerically analysed. Furthermore, different substrate materials were considered so a wider range of bonded joints could be studied, i.e., CFRP-to-concrete [78], CFRP-to-steel [79], and CFRP-to-brick joints [80].

4.1. Tests carried out by Borba [78]

The single-lap shear tests of CFRP-to-concrete bonded joints carried out by Borba [78] were considered. In these tests, the cross-sectional area of the CFRP composite is 1.4×10 mm^2 (thickness×width) with average mechanical properties as follows: elastic modulus of 159 GPa, a tensile strength of 1,565 MPa and rupture strain of 1.03%. The dimensions of the concrete blocks are 300×300×650 mm^3 (thickness×width×length) with an average compression strength of 22.7 MPa with an elastic modulus of 28.1 GPa. The CFRP composite was externally bonded to the concrete's surface with epoxy resin S&P220, which has a brittle behaviour. Different bonded lengths of 50 mm, 100 mm, 150 mm, and 300 mm were also considered. The local bond behaviour was approximated by Borba [78] with the exponential bond-slip relationship defined in Eq. (1) where the following parameters were obtained from two tests with a bonded length of 300 mm: $\tau_{b\max} = 10.19$ MPa, $B = 10.830$ mm^{-1} and $G_F = 1.882$N/mm.

In addition to the experimental work, Borba [78] developed an analytical solution that can predict the bond behaviour of the CFRP-to-concrete joints. That analytical solution is based on the exponential bond-slip relationship defined in Eq. (1) and it can be used only with FRP-to-substrate bonded joints with no mechanical anchorages or mixed-adhesive joints. So, despite the interest, the analytical solution proposed by Borba [78] is quite limited when compared with the analytical solution proposed in this work.

In Fig. 11, the load-slip curves predicted by the proposed analytical solution are compared with the experimental and analytical data reported by Borba [78]. As can be seen from Fig. 11, the load-slip curves obtained from the proposed analytical solution are very accurate with the analytical results obtained by Borba [78]. However, when the equilibrium condition defined in Eq. (28) is used to predict the load-slip curve, the maximum loads transmitted to the CFRP composite are slightly underestimated, especially in those cases with the lowest bonded lengths. Particularly in specimens with $L_b = 50$ mm, the load-slip curve obtained from the proposed analytical model underestimates the load-slip curve obtained from the analytical model developed by Borba [78]. Also, using the equilibrium condition stated in Eq. (28) the maximum load predicted of 4.67 kN underestimates by 14.6% the experimental result that led to an average value of 5.47 kN.

The specimens tested by Borba [78] were now modified. Thus, a ductile adhesive was used as an additional anchorage and the same bonded length was kept unchanged. For simplicity, the specimen with a bonded length of 300 mm was considered and two anchorage lengths of 50 mm and 150 mm were used, which represent one-sixth and one-half of the bonded length, respectively. Two positions of this ductile adhesive anchorage, i.e. close to the CFRP unpulled and loaded ends, were also considered. A single-adhesive bonded joint with a ductile adhesive and bonded length of 300 mm was also assumed as a reference purpose. For convenience, the same ductile

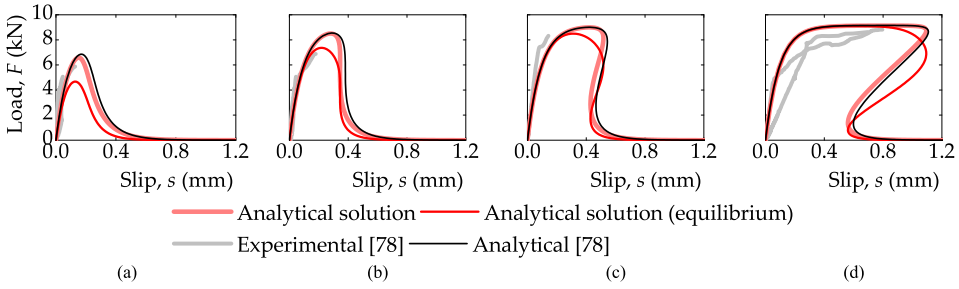

Fig. 11. Comparison between the load-slip curves obtained from the proposed analytical solution with the experimental and analytical results obtained by Borba [78] for the CFRP-to-concrete joints with bonded lengths of: (a) 50 mm; (b) 100 mm; (c) 150 mm; and (d) 300 mm.

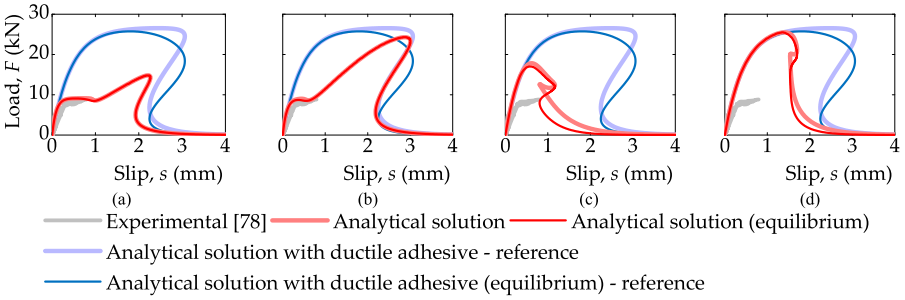

Fig. 12. Influence of the use of a ductile adhesive as an additional anchorage in the experiments of Borba [78] with a length of: (a) 50 mm close to the CFRP unpulled end; (b) 150 mm close to the CFRP unpulled end; (c) 50 mm close to the CFRP loaded end; and (d) 150 mm close to the CFRP loaded end.

adhesive described in subsection 2.2 was used. The load-slip curves obtained from the proposed analytical solution are presented in Fig. 12. The results show that using the ductile adhesive with the longest length of 100 mm regardless of its positioning, i.e. as an end or loaded-end anchorage, leads to the highest load capacities. Thus, using the ductile adhesive as an end anchorage, the maximum load predicted by the analytical solution is 24.29 kN, whereas by using the ductile adhesive as a loaded-end anchorage a maximum load of 25.48 kN was estimated. Nevertheless, it can be also seen that if the ductile adhesive is used throughout the full length of the bonded length, i.e. assuming a single-adhesive joint, the load capacity is 26.54 kN, which represents the highest maximum load capacity of the joint. Therefore, in terms of the strength increase of the joints, these results suggest that the use of a mixed adhesive joint idea is useless when compared with the single-adhesive joint with a ductile adhesive.

4.2. *Tests carried out by Silva [79]*

The aim of the study carried out by Silva [79] was to understand the bond behaviour of CFRP-to-steel joints. The work [79] follows an experimental programme with CFRP composites externally bonded to a rectangular hollowed steel profile with different bonded lengths of 50 mm, 75 mm, 100 mm, 150 mm, 175 mm and 200 mm. Silva [79] used the same CFRP composite and adhesive used by Borba [78]. The steel was not tested but Silva [79] considered an elastic modulus of 200 GPa. The rectangular hollowed section has 100 mm of side, a thickness of 10 mm and a length of 500 mm. Like Borba [78], Silva [79] adjusted the experimental bond-slip curve to the exponential function defined in Eq. (1) and used the same analytical model proposed by Borba [78] to predict the experimental results. In this case of the CFRP-to-steel joints, the following parameters to define the average bond-slip relationship are: $\tau_{bmax} = 9.29$ MPa, $B = 12.260$ mm^{-1} and $G_F = 1.520$N/mm.

The load-slip curves obtained from the analytical solution are compared with the experimental and analytical predictions carried out by Silva [79] in Fig. 13. The results obtained from the proposed analytical solution are similar to those obtained from the analytical model. Like in the specimen with the shortest bonded length tested by Borba [78], the proposed analytical solution underestimates the

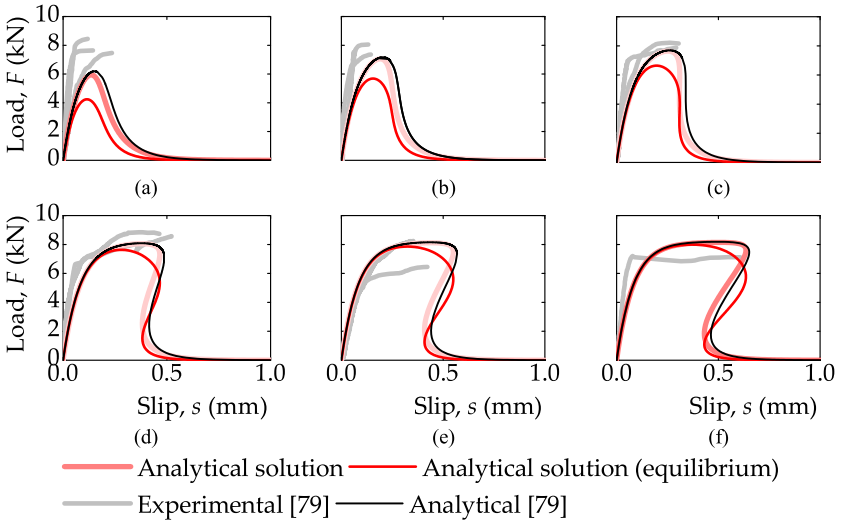

Fig. 13. Comparison between the load-slip curves obtained from the proposed analytical solution with the experimental and analytical results obtained by Silva [79] for the CFRP-to-concrete joints with bonded lengths of: (a) 50 mm; (b) 75 mm; (c) 100 mm; (d) 150 mm; (e) 175 mm; and (f) 200 mm.

analytical results of the specimen with $L_b = 50$ mm. However, the analytical solution leads to underestimating the load capacity. From the equilibrium condition in (28), the predicted maximum load capacity is 4.67 kN, which is 40.5% lower than the average maximum load value (7.85 kN) obtained from the experiments and it represents the highest deviation found. This difference can be attributed to the definition of the parameters used in the bond-slip relationship, which average used here is different from the average values of these particular tests. Nevertheless, within an overall overview of the load-slip curves, the proposed analytical solution can estimate, with fair accuracy, the experimental and analytical results reported by Silva [79].

The same rationale used for the specimen with the longest bonded length tested by Borba [78] was followed here also, i.e., an additional anchorage with a ductile adhesive was added to the specimens with a bonded length of 200 mm. Then, the influence of this anchorage as well as its positioning were both analysed. Fig. 14 shows the load-slip curves obtained by the proposed analytical solution. Like the predictions made for the CFRP-to-concrete joints tested by Borba [78], these results also suggest that the use of a mixed-adhesive joint cannot increase the load capacity of the single-adhesive joint with a ductile adhesive. Also, the highest load capacities of the mixed-adhesive joints were reached when a 100 mm length was used. When the ductile adhesive was used as a loaded-end anchorage, the maximum load transmitted to the CFRP composite reached 22.74 kN, which is 11.3% lower than the reference single-adhesive joint that had a maximum load of 25.63 kN. The use of the loaded-end anchorage also decreases the ductility (in displacement) of the joint (see, e.g., Fig. 14d). However, when the ductile adhesive is used as an end anchorage, the ductility of the joint is almost unchanged but the maximum load decreased to 20.99 kN, which is 18.1% lower than the maximum load of the single-adhesive joint with the ductile adhesive. Moreover, the load-slip curves of the mixed-adhesive joints with an end anchorage show three stages until the maximum load is reached (see Fig. 14a and 14b). Thus, the two first stages are due to the debonding process of the brittle adhesive, whereas the third corresponds to the debonding process of the ductile adhesive. As the length of the ductile adhesive increases the slope of this third stage increases and it has more influence on the load capacity of the joint.

4.3. Tests carried out by Zhang et al. [80]

Zhang et al. [80] studied the influence of dynamic loading on the local bond adherence of CFRP-to-brick joints. The CFRP sheets were externally bonded to the bricks with epoxy resin HM-180C3P, which is a bi-component fibre adhesive produced by Horse China for structural reinforcement and it has a brittle behaviour. The nominal layer of the CFRP sheets is 0.167 mm and has an elastic modulus equal to 253 GPa, with a tensile strength of 4000 MPa and a rupture strain of 1.7%. The bricks were made of clay and had $240\times115\times53$ mm^3 (length×width×thickness). The tensile and compression strengths of the clay bricks are 2.85 MPa and 11.4 MPa, respectively, and an elastic modulus of 7.6 GPa. The specimens had a bonded length of 160 mm and a CFRP width of 40 mm. The single-lap shear tests of the CFRP-to-brick bonded joints showed that the bond-slip relationship can be approximated to an exponential function similar to Eq. (1). For simplicity, specimen A4 (under a loading rate of 10 mm/min) is the unique specimen replicated here and, therefore, the parameters needed to define Eq. (1) are as follows: $\tau_{b\max} = 3.46$ MPa, $B = 11.744$ mm^{-1}, and $G_F = 0.592$N/mm.

The experimental load-slip curve of specimen A4 obtained by Zhang et al. [80] is shown in Fig. 15a. In this figure, the results obtained from the proposed analytical solution are also shown. Despite some differences on the ascending branch of the load-slip curve, the maximum load is well predicted. Six points were also highlighted in the load-slip curves obtained from the analytical solution, i.e. at the interfacial slips at the CFRP loaded end of 0.036 mm (Point *A*), 0.061 mm (Point *B*), 0.102 mm (Point *C*), 0.250 mm (Point *D*), 0.442 mm (Point *E*), and 0.533 mm (Point *F*). The corresponding CFRP strain distributions of those six points are presented in Fig. 15b where the results of the analytical solution are compared with those obtained experimentally by Zhang et al. [80]. As can be seen from Fig. 15b, the CFRP strains obtained from the analytical results follow the experimental data closely.

Fig. 16 aims to show the load capacities of the CFRP-to-brick bonded joints if a ductile adhesive was used as an additional anchorage. The results are also compared with the case of a single-adhesive joint with a ductile adhesive for reference purposes. Thus, four additional different situations were considered. The first and second cases, whose results are shown in Fig. 16a and 16b, consist, respectively, of a bonded anchorage of 25 mm and 135 mm in length with the ductile adhesive placed close to the CFRP unpulled end.

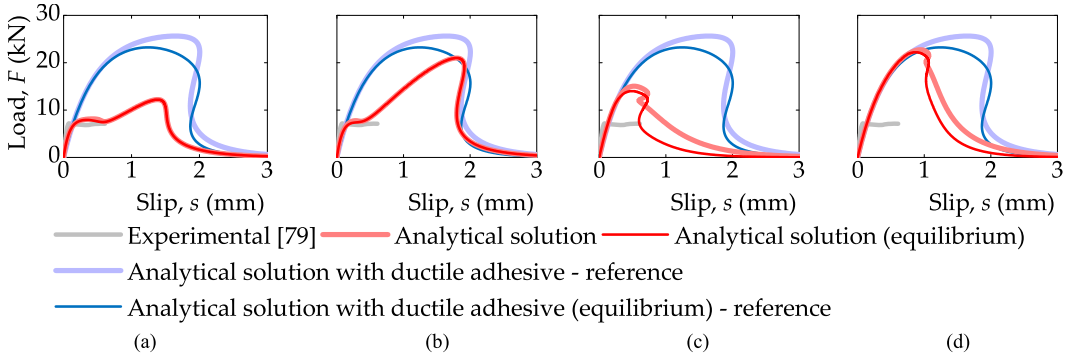

Fig. 14. Influence of the use of a ductile adhesive as an additional anchorage in the experiments of Silva [79] with a length of: (a) 35 mm close to the CFRP unpulled end; (b) 100 mm close to the CFRP unpulled end; (c) 35 mm close to the CFRP loaded end; and (d) 100 mm close to the CFRP loaded end.

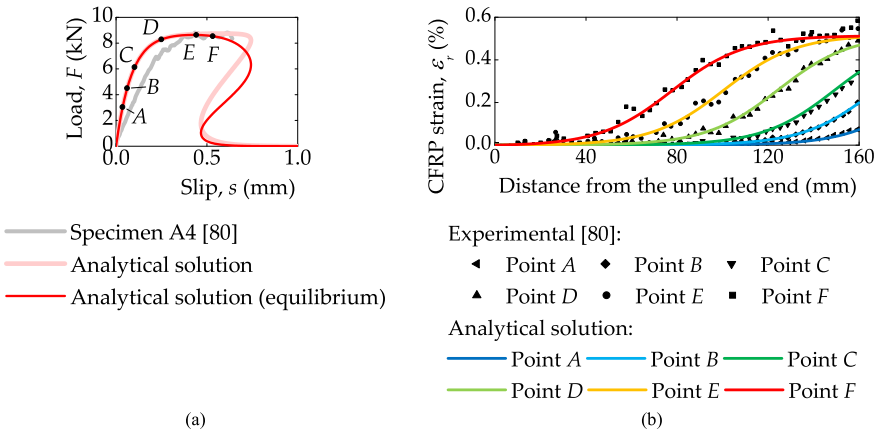

Fig. 15. Comparison between the analytical solution with the experimental results of specimens A4 tested by Zhang et al. [80]: load-slip curve; and (b) CFRP strain configuration.

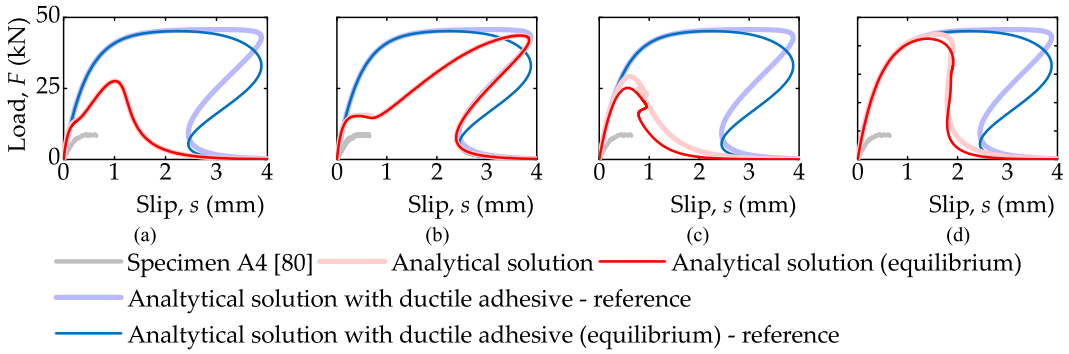

Fig. 16. Influence of the use of a ductile adhesive as an additional anchorage in the experiments of Zhang et al. [80] with a length of: (a) 25 mm close to the CFRP unpulled end; (b) 80 mm close to the CFRP unpulled end; (c) 25 mm close to the CFRP loaded end; and (d) 80 mm close to the CFRP loaded end.

In alternative to these two first cases, the bonded anchorage with the ductile adhesive was shifted to the CFRP-loaded end with the same bonded lengths, i.e. 25 mm and 135 mm (see Fig. 16c and 16d, respectively). The results confirm the results obtained from the CFRP-to-concrete and CFRP-to-steel joints tested by Borba [78] and Silva [79], respectively. Thus, the single-adhesive joint with the ductile adhesive had the highest load capacity (45.71 kN) and ductility. Moreover, the mixed-adhesive joints with the longest ductile length led to the highest load capacities of 43.64 kN and 44.03 kN in the specimens with the end and loaded-end anchorages, respectively. However, the ductility of the specimen with the load-end anchorage was reduced while the ductility of the specimen with the end anchorage was kept unchanged.

5. Conclusions

This work aims to propose a new analytical solution that predicts the nonlinear behaviour of mixed-adhesive bonded joints and mitigates the lack of knowledge of their bond performance. The efficiency of using this bonding technique was studied by adopting different bonded lengths and configurations. The proposed analytical solution was mainly validated by comparing the load-slip curves with those obtained from the FEM. Since no data was found in the literature, the bond behaviour of CFRP-to-concrete, CFRP-to-steel, and CFRP-to-timber bonded joints found in the literature with a ductile adhesive as an additional anchorage was also predicted. Based on all the results achieved in this work, the main following conclusions can be drawn:

- The proposed analytical solution is simple to use and can predict the bond performance of FRP composites externally bonded to a structural material. Its wide application covered the debonding prediction, with good accuracy, of different mixed-adhesive joints, i.e. combining a ductile and brittle adhesive throughout the bond line of the joint;
- The prediction of bonded joints with a short-bonded length tends to underestimate the load capacities of the joints numerically simulated with the FEM. For instance, in the case of specimen CS-L100A, the analytical model overestimated the maximum load of

the specimen by approximately 23.3%. However, as the bonded length increases, the maximum loads transmitted to the joints are well predicted. Until the snapback phenomenon, the IAE values were all lower than 10%;

- When the equilibrium condition of the mixed-adhesive joint is used, the maximum loads transmitted to the CFRP composite tend to be slightly lower than that predicted by Eqs. (17) and (19). Nevertheless, for mixed-adhesive joints with long bonded lengths, such difference is marginal and the same result is obtained;
- The idea of using a mixed-adhesive joint as an alternative to a ductile single-adhesive joint seems to be ineffective. The use of a single-adhesive joint with a ductile adhesive leads to the highest load capacities than any of the other cases herein studied with mixed-adhesive joints. Still, using the ductile adhesive as an end and loaded-end anchorage led to different load-slip curves with different maximum loads and ductilities. Thus, for the same anchorage length, using the ductile adhesive on the side of the CFRP-loaded end (as a loaded-end anchorage) lead to higher maximum loads than in the opposite case, i.e., using a ductile adhesive as an end anchorage. Although not calculated, the ductility of the joint with the loaded-end anchorage is visibly reduced, whereas, with the end anchorage, the ductility is reduced only in the joints with a short length end anchorage.

Due to the possibility of adopting a nonlinear spring, the proposed analytical model can be used also to predict the bond behaviour of other cases with other anchorage types, such as the use of CFRP spike anchors, steel plate, a wider CFRP composite, or any other commercial anchorage. Therefore, the proposed analytical solution may open a new research topic towards the understanding of the influence of other anchorage types on the bond performance of FRP-to-substrate bonded joints by using the same analytical solution. For all these reasons, the proposed design-oriented equations have a large potential use by other researchers or engineers working in the area of the strengthening of structures with FRP composites.

CRediT authorship contribution statement

Hugo C. Biscaia: Writing – original draft, Validation, Supervision, Software, Project administration, Methodology, Investigation, Funding acquisition, Formal analysis, Data curation, Conceptualization. **Dilum Fernando:** Writing – review & editing, Validation, Investigation. **Jian-Guo Dai:** Writing – review & editing, Validation, Investigation.

Declaration of competing interest

The authors declare the following financial interests/personal relationships which may be considered as potential competing interests: Hugo C. Biscaia reports financial support was provided by Foundation for Science and Technology.

Jian-Guo Dai reports financial support was provided by City University of Hong Kong Startup Funding “Advanced Functional Construction Materials (AFCM) for Sustainable Built Environment” (Project code: 9380165). Dilum Fernando reports no competing financial interests or personal relationships that could have appeared to influence the work reported in this paper..

Acknowledgments

The authors are thankful to Fundação para a Ciência e Tecnologia (FCT-MCTES) for the partial funding of this work under the strategic projects UIDP/00667/2020 and UIDB/00667/2020 as well as City University of Hong Kong Startup Funding “Advanced Functional Construction Materials (AFCM) for Sustainable Built Environment” (Project code: 9380165).

Data availability

Data will be made available on request.

References

[1] da Silva LFM, Lopes MJCQ. Joint strength optimization by the mixed-adhesive technique. Int J Adhes Adhes 2009;29(5):509–14.
[2] da Silva, LFM (2010). Technology of mixed adhesive joints. In: da Silva, L., Pirondi, A., Öchsner, A. (eds) Hybrid Adhesive Joints. Advanced Structured Materials, vol 6. Springer, Berlin, Heidelberg.
[3] Vallée T, Tannert T, Murcia-Delso J, Quinn DJ. Influence of stress-reduction methods on the strength of adhesively bonded joints composed of orthotropic brittle adherends. Int J Adhes Adhes 2010;30(7):583–94.
[4] Chiminelli A, Breto R, Izquierdo S, Bergamasco L, Duvivier E, Lizaranzu M. Analysis of mixed adhesive joints considering the compaction process. Int J Adhes Adhes 2017;76:3–10.
[5] Kaufmann M, Vallée T. Topology optimization of adhesively bonded double lap joints. Int J Adhes Adhes 2022;118:103238.
[6] Lang TP, Mallick PK. Effect of spew geometry on stresses in single lap adhesive joints. Int J Adhes Adhes 1997;18:167–77.
[7] Machado JJM, Gamarra PMR, Marques EAS, da Silva LFM. Numerical study of the behaviour of composite mixed adhesive joints under impact strength for the automotive industry. Compos Struct 2018;185:373–80.
[8] Ramezani F, Ayatollahi MR, Akhavan-Safar A, da Silva LFM. A comprehensive experimental study on bi-adhesive single lap joints using DIC technique. Int J Adhes Adhes 2020;102:102674.
[9] Wei Y, Jin X, Luo Q, Li Q, Sun G. Adhesively bonded joints - A review on design, manufacturing, experiments, modeling and challenges. Compos B Engng 2024;276:111225.
[10] Raphael C. Variable-adhesive bonded joints. Appl Polymer Symposium 1966;3:99–108.
[11] Crocombe AD, Adams RD. Influence of the spew fillet and other parameters on the stress distribution in the single lap joint. J Adhes 1981;13(2):141–55.
[12] Frostig Y, Thomsen OT, Mortensen F. Analysis of adhesive-bonded joints, square-end, and spew-fillet-high order theory approach. J Engng Mech 1999;125(11):1298–307.

[13] Mortensen F, Thomsen OT. Analysis of adhesive bonded joints: a unified approach. Compos Sci Technol 2002;62(7–8):1011–31.
[14] Akpinar S, Doru MO, Özel A, Aydin MD, Jahanpasand HG. The effect of the spew fillet on an adhesively bonded single-lap joint subjected to bending moment. Compos B Engng 2013;55:55–64.
[15] dos Reis MQ, Marques EAS, Carbas RJC, da Silva LFM. Functionally graded adherends in adhesive joints: An overview. J Adv Joining Process 2020;2:100033.
[16] Belingardi G, Goglio L, Tarditi A. Investigating the effect of spew and chamfer size on the stresses in metal/plastics adhesive joints. Int J Adhes Adhes 2002;22:273–82.
[17] Kaye R, Heller M. Through-thickness shape optimisation of typical double lap-joints including effects of differential thermal contraction during curing. Int J Adhes Adhes 2005;25:227–38.
[18] Pethrick RA. Design and ageing of adhesives for structural adhesive bonding – a review. Proc Instit Mech Eng, Part L: J Mater: Design Appl 2015;229(5):349–79.
[19] Kupski J, de Freitas ST. Design of adhesively bonded lap joints with laminated CFRP adherends: review, challenges and new opportunities for aerospace structures. Compos Struct 2021;268:113923.
[20] Zhao X, Adams RD, da Silva LFM. Single lap joints with rounded adherend corners: Stress and strain analysis. J Adhes Sci Technol 2011;25(8):837–56.
[21] Bouchikhi AS, Megueni A, Gouasmi S, Boukoulda FB. Effect of mixed adhesive joints and tapered plate on stresses in retrofitted beams bonded with a fiber-reinforced polymer plate. Mater Des 2013;50:893–904.
[22] Zhao B, Lu ZH, Lu YN. Closed-form solutions for elastic stress-strain analysis in unbalanced adhesive single-lap joints considering adherend deformations and bond thickness. Int J Adhes Adhes 2011;31(6):434–45.
[23] Amidi S, Wang J. An analytical model for interfacial stresses in double-lap bonded joints. J Adhes 2019;95(11):1031–55.
[24] Her SC, Chan CF. Interfacial stress analysis of adhesively bonded lap joint. Materials 2019;12(15):2403.
[25] Nguyen TH, Le Grognec P. Analytical and numerical simplified modeling of a single-lap joint. Int J Adhes Adhes 2021;108:102827.
[26] Li A, Wang H, Li H, Kong D, Xu S. Estimation of bond strength and effective bond length for the double strap joint between carbon fiber reinforced polymer (CFRP) plate and corroded steel plate. Polymers 2022;14(15):3069.
[27] Hart-Smith LJ, Adhesive bonded double lap joints. 1973: p. NASA CR-112235.
[28] Biscaia HC, Chastre C, Silva MAG. A smeared crack analysis of reinforced concrete T-beams strengthened with GFRP composites. Engng Struct 2013;56:1346–61.
[29] Biscaia HC, Chastre C, Silva MAG. Analytical model with uncoupled adhesion laws for the bond failure prediction of curved FRP-concrete joints subjected to temperature. Theor Appl Fract Mech 2017;89:63–78.
[30] de Carvalho NV, Mabson GE, Krueger R, Deobal LRA. New approach to model delamination growth in fatigue using the virtual crack closure technique without re-meshing. Engng Fract Mech 2019;222:106614.
[31] Asm AA, Kawashita LF, Featherston CAA. Modified cohesive zone model for fatigue delamination in adhesive joints: numerical and experimental investigations. Compos Struct 2019;225:111114.
[32] Choi YH, Kim HG. Development of a cohesive zone model for fatigue crack growth. Multiscale Sci Engng 2020;2:42–53.
[33] Rocha AVM, Akhavan-Safar A, Carbas R, Marques EAS, Goyal R, El-zein M, et al. Numerical analysis of mixed-mode fatigue crack growth of adhesive joints using CZM. Theor Appl Fract Mech 2020;106:102493.
[34] Tserpes K, Barroso-Caro A, Carraro PA, Beber VC, Floros I, Gamon W, et al. A review on failure theories and simulation models for adhesive joints. J Adhes 2022;98(12):1855–915.
[35] Akhavan-Safar A, Marques EAS, Carbas RJC, da Silva LFM. Cohesive zone modelling-CZM. Cohesive Zone Modelling for Fatigue Life Analysis of Adhesive Joints. SpringerBriefs in Applied Sciences and Technology. Cham: Springer; 2022.
[36] He J, Xian G, Zhang YX. Numerical modelling of bond behaviour between steel and CFRP laminates with a ductile adhesive. Int J Adhes Adhes 2021;104:102753.
[37] Zhao J, Fang J, Yang Y, Zhang S, Biscaia H. Experimental study on mixed mode-I & II bond behavior of CFRP-to-steel joints with a ductile adhesive. Thin-Walled Struct 2023;184:110532.
[38] Biscaia H, Coelho P, Conde F, D'Antino T. Theoretical study on the bond performance of CFRP-to-steel single-lap shear tests with multiple debonding defects. Compos Struct 2024;345:118406.
[39] Yuan H, Teng JG, Seracino R, Wu ZS, Yao J. Full-range behavior of FRP-to-concrete bonded joints. Engng Struct 2004;26(5):553–65.
[40] Teng JG, Yuan H, Chen JF. FRP-to-concrete interfaces between two adjacent cracks: Theoretical model for debonding failure. Int J Solids Struct 2006;43(18–19):5750–78.
[41] Fernando D, Yu T, Teng JG. Behavior of CFRP laminates bonded to a steel substrate using a ductile adhesive. J Compos Constr 2013;18(2):04013040.
[42] Biscaia HC, Franco N, Chastre C. Development of a simple bond-slip model for joints monitored with the DIC technique. Arch Civ Mech Engng 2018;18:1535–46.
[43] Milani G, Grande E, Bertolesi E, Rotunno T, Fagone M. Debonding mechanism of FRP strengthened flat surfaces: Analytical approach and closed form solution. Constr Build Mater 2021;302:124144.
[44] Martinelli E. (2021). Closed-form solution procedure for simulating debonding in FRP strips glued to a generic substrate material. Fibers 2021, 9(4):22.
[45] Biscaia H, Carvalho M, Martins AP, Micaelo R. Interfacial failure of circular or tubular hybrid bonded joints: a theoretical description. Engng Fail Anal 2022;132:105936.
[46] Biscaia HC. The influence of temperature variations on adhesively bonded structures: A non-linear theoretical perspective. Int J Non Linear Mech 2019;113:67–85.
[47] Biscaia HC. Closed-form solutions for modelling the response of adhesively bonded joints under thermal loading through exponential softening laws. Mech Mater 2020;148:103527.
[48] Guo D, Zhou H, Wang HP, Dai JG. Effect of temperature variation on the plate-end debonding of FRP-strengthened steel beams: Coupled mixed-mode cohesive zone modeling. Engng Fract Mech 2022;270:108583.
[49] Biscaia H, Martins AP, Gao WY, Carvalho MS. Influence of uniform temperature variations on hybrid bonded joints with a circular or tubular cross-sectional area. Mech Mater 2023;179:104600.
[50] Guo D, Liu YL, Gao WY, Dai JG. Bond behavior of CFRP-to-steel bonded joints at different service temperatures: experimental study and FE modelling. Constr Build Mater 2023;362:129836.
[51] Gao WY, Teng JG, Dai JG. Effect of temperature variation on the full-range behavior of FRP-to-concrete bonded joints. J Compos Constr 2012;16(6):671–83.
[52] Zhou H, Gao WY, Biscaia HC, Wei XJ, Dai JG. Debonding analysis of FRP-to-concrete interfaces between two adjacent cracks in plated beams under temperature variations. Engng Fract Mech 2022;263:108307.
[53] Dai J, Ueda T, Sato Y. Unified analytical approaches for determining shear bond characteristics of FRP-concrete interfaces through pullout tests. J Adv Concr Technol 2006;4(1):133–45.
[54] Jiang C, Yu QQ, Gu XL. A unified bond-slip model for the interface between FRP and steel. Compos B Engng 2021;227:109380.
[55] Ke L, Li C, Luo N, He J, Jiao Y, Liu Y. Enhanced comprehensive performance of bonding interface between CFRP and steel by a novel film adhesive. Compos Struct 2019;229:111393.
[56] Biscaia H, Carmo N. Bond assessment between rebars embedded into a parent material using a single-function bond-slip model. Constr Build Mater 2023;397:132396.
[57] Wang HT, Wu G, Dai YT, He XY. Determination of the bond–slip behavior of CFRP-to-steel bonded interfaces using digital image correlation. J Reinf Plast Compos 2016;35(18):1353–67.
[58] Yu T, Fernando D, Teng JG, Zhao XL. Experimental study on CFRP-to-steel bonded interfaces. Compos B Engng 2012;43(5):2279–89.
[59] Lu T, Li P, Cui C, Wu J, Fu B. Shear transferring mechanism of the FPR-to-concrete bonded joint with end U-jacketing: A theoretical study. Structures 2023;56:104991.

[60] Caggiano A, Martinelli E, Faella C. A fully-analytical approach for modelling the response of FRP plates bonded to a brittle substrate. Int J Solids Struct 2012;49 (17):2291–300.
[61] Gao WY, Dai JG, Teng JG. Analysis of Mode II debonding behavior of fiber-reinforced polymer-to-substrate bonded joints subjected to combined thermal and mechanical loading. Engng Fract Mech 2015;136:241–64.
[62] Yang Y, Biscaia H, Chastre C, Silva MAG. Bond characteristics of CFRP-to-steel joints. J Constr Steel Res 2017;138:401–19.
[63] Nelson LA, Al-Allaf M, Weekes L. Analytical modelling of bond-slip failure between epoxy bonded FRP and concrete substrate. Compos Struct 2020;251:112596.
[64] Biscaia HC, Canejo J, Zhang S, Almeida R. Using digital image correlation to evaluate the bond between carbon fibre-reinforced polymers and timber. Struct Health Monit 2021:1–24.
[65] Cervenka V, Jendele L, Cervenka J. ATENA Program Documentation – Part 1 – Theory. Prague: Cervenka Consulting; 2021.
[66] Wu YF, Zhao XM. Unified bond stress-slip model for reinforced concrete. J Struct Engng 2013;139(11):1951–62.
[67] Shen D, Shi X, Ji Y, Yin F. Strain rate effect on bond stress-slip relationship between basalt fiber-reinforced polymer sheet and concrete. J Reinf Plast Compos 2015;34(7):547–63.
[68] Carvalho T, Chastre C, Biscaia H, Paula R. Flexural behaviour of RC T-beams strengthened with different FRP materials. Third International fib Congress Washington, May-June, 2010.
[69] Kowal M, Rozylo P. Effect of bond end shape on CFRP/steel joint strength. Compos Struct 2022;284:115186.
[70] Biscaia HC, Micaelo R. Emerging anchored FRP systems bonded to steel subjected to monotonic and cyclic loading: A numerical study. Engng Fract Mech 2022; 261:108250.
[71] Zhang SS, Ke Y, Chen E, Biscaia H, Li WG. Effect of load distribution on the behaviour of RC beams strengthened in flexure with near-surface mounted (NSM) FRP. Compos Struct 2022;279:114782.
[72] Rozylo P. Failure phenomenon of compressed thin-walled composite columns with top-hat cross-section for three laminate lay-ups. Compos Struct 2023;304: 116381.
[73] Huang Y, Cui C, Tian K, Wu J. Closed-form solutions for FPR-to-concrete bonded joints with loaded-end anchorage: Insight into the interfacial shear transferring mechanism. Structures 2024;66:106807.
[74] Biscaia HC, Chastre C, Silva MAG. Bond-slip model for FRP-to-concrete bonded joints under external compression. Compos B Engng 2015;80:246–59.
[75] Biscaia H, Chastre C. Design method and verification of steel plate anchorages for FRP-to-concrete bonded interfaces. Compos Struct 2018;192:52–66.
[76] Zhang H, Smith ST, Gravina RJ, Wang Z. Modelling of FRP-concrete bonded interfaces containing FRP anchors. Constr Build Mater 2017;139:394–402.
[77] Colalillo MA, Sheikh SA. Behaviour of shear-critical RC beams strengthened with FRP - Experimentation. Structural Journal 2023;111(6):1373–84.
[78] Borba IS. (2015) Comportamento da ligação CFRP/betão em estruturas de betão armado. MSc thesis, NOVA School of Science and Technology, Universidade NOVA de Lisboa, 2015. [In Portuguese].
[79] Silva CP. (2015). Comportamento de ligações adesivas entre compósitos de FRP e elementos estruturais de aço. MSc Thesis, NOVA School of Science and Technology, Universidade NOVA de Lisboa. [In Portuguese].
[80] Zhang D, Yang J, Chi LY. The bond-slip relationship at FRP-to-brick interfaces under dynamic loading. Materials 2021;14:545.